

Marquette University
e-Publications@Marquette

Master's Theses (2009 -)

Dissertations, Theses, and Professional Projects

Investigation of Reactive Oxygen Species Production in the Rat Lung Using Optical Imaging

Nina Friedly
Marquette University

Recommended Citation

Friedly, Nina, "Investigation of Reactive Oxygen Species Production in the Rat Lung Using Optical Imaging" (2018). *Master's Theses (2009 -)*. 470.
https://epublications.marquette.edu/theses_open/470

Investigation of Reactive Oxygen Species Production
in the Rat Lung Using Optical Imaging

By

Nina Friedly, B.S.

A Thesis submitted to the Faculty of the Graduate School, Marquette University, in
Partial Fulfillment of the Requirements for the Degree of Master of Science

Milwaukee, Wisconsin

May 2018

ABSTRACT

Investigation of Reactive Oxygen Species Production in the Rat Lung Using Optical Imaging

Nina Friedly, B.S.

Marquette University, 2018

Oxidative stress, the imbalance between production of oxidants or reactive oxygen species (ROS) and antioxidant activity, plays a key role in the pathogenesis of acute and chronic lung diseases. The objective of this thesis was to develop a robust protocol for measuring the rate of H_2O_2 production in isolated perfused rat lungs and to determine the cellular sources of that rate using Amplex Red (AR).

For a given lung, AR (25 mM) along with horseradish peroxidase (5 U/ml) and ascorbate oxidase (1U/ml) were added to a perfusate reservoir that was recirculated through the lungs and sampled at 5 minute intervals to measure the emission signal (454 nm/610 nm). Experiments were carried without and with the inhibitors rotenone (40 μ M), thenoyltrifluoroacetone (20 μ M), antimycin A (3.76 μ M), potassium cyanide (2 mM), or dihenylene iodonium (5 μ M) added to the recirculating perfusate. In addition, we evaluated the effect of % O_2 ventilation on H_2O_2 production.

For lungs from control rats, the results show that inhibiting mitochondrial complex II reduced this rate by $76 \pm 3\%$, and inhibiting NOX reduced it by another $23 \pm 2\%$. The results also show that inhibiting complex I had a small ($13\% \pm 4\%$), but significant effect on the rate, whereas inhibiting complex III had no significant effect on this rate. Inhibition of complex IV increased the rate or ROS production by $310\% \pm 43\%$. Furthermore, the results show that increasing % O_2 in the ventilation gas mixture from 15% to 95% O_2 had a relatively small ($27 \pm 3\%$), but significant effect on this rate, and that this O_2 -dependent increase was mostly non-mitochondrial.

The results of this study suggest complex II as a potentially important source of ROS and a potential target for mitigating oxidative stress, and that most of the hyperoxia-enhanced lung rate H_2O_2 release is from NAD(P)H oxidase rather than mitochondrial sources. To the best of our knowledge, this is the first study measuring the rate of H_2O_2 release from isolated perfused rat lungs, identifying the main sources of this rate under physiological conditions, and evaluating the effect of acute hyperoxia on this rate.

ACKNOWLEDGMENTS

Nina Friedly, B.S.

I dedicate this dissertation to my family members and partner, who have been there for me through it all. Much of this work would not have been possible without my partner and family members that made me who I am today and supported me through the tough times.

I would also like to thank my advisor, Dr. Said Audi, whose mentorship and expertise have made my studies possible. His guidance through school has been essential since the day I started my academic career at Marquette University. Sincere thanks to Dr. Anne Clough, Dr. Elizabeth Jacobs, and Dr. Ranjan Dash for serving on this thesis committee. I would also like to extend my gratitude to Carlos Marquez-Barrientos and Dr. Steven Haworth for their help with the experiments.

I thank Marquette University for the opportunity to earn my Bachelor's and Master's degrees and to work on this project. Finally, for anyone who has contributed, directly and indirectly, to the completion of this thesis, I extend my appreciation.

TABLE OF CONTENTS

ABSTRACT.....	i
ACKNOWLEDGEMENTS	ii
LIST OF TABLES.....	v
LIST OF FIGURES	vi
CHAPTER 1: INTRODUCTION, BACKGROUND, AND OBJECTIVE	1
1.1 Clinical Motivation.....	1
1.2 Oxidative Stress: Reactive Oxygen Species (ROS), Antioxidant Mechanisms, and Cellular Sources of ROS	2
1.3 Methods for Measuring Cellular Rate of ROS Production.....	9
1.4 Considerations for H ₂ O ₂ Measurement with AR.....	12
1.5 Pharmacological Approach for Determining the Sources ROS Sources	14
1.6 Objective.....	16
CHAPTER 2: EXPERIMENTAL METHODS.....	18
2.1 Materials	18
2.2 Isolated, Perfused Rat Lung Preparation	18
2.3 Optical Fluorescent Imaging System.....	19
2.4 Experimental Protocols.....	20
2.4.1 Lung-Independent Rate of AR Conversion to Resorufin	23
2.4.2 Standard Curve Procedure	24
CHAPTER 3: DATA ANALYSIS	25
3.1 Standard Curve.....	25
3.2 Lung Data.....	26

3.3 Statistical Analysis.....	28
CHAPTER 4: RESULTS	29
4.1 Rats Body Weights, Lung Wet Weights, Dry Weights, and Wet-to-Dry Weight Ratios, and Pulmonary Artery Pressures	29
4.2 Resorufin Standard Curves Without and With Mitochondrial and NOX Inhibitors	30
4.3 Amplex Red Auto-Oxidation Rate	33
4.4 Lung Rate of H ₂ O ₂ Release and the Contributions of Mitochondria and NOX to this Rate	34
4.5 Effects of Mitochondrial/NOX Inhibitor Vehicles on Measured Rates of Lung H ₂ O ₂ Release.....	37
4.6 Effect of O ₂ Level in Ventilation Gas on the Lung Rate of H ₂ O ₂ Release	38
CHAPTER 5: DISCUSSION	40
5.1 Interpretation of Results.....	40
5.2 Limitations of AR in the Isolated, Perfused Lung Preparation.....	49
5.3 Conclusions.....	51
BIBLIOGRAPHY	52
APPENDICES	58

LIST OF TABLES

Table 1.1 Mitochondrial ETC complex inhibitors and their targets	15
Table 4.1 Body weight, lung wet weight, dry lung weight, and wet-to-dry weight ratio for each of the experimental conditions	29
Table A.1 List of inhibitors.....	61

LIST OF FIGURES

Figure 1.1 Progression of ALI/ARDS	1
Figure 1.2 Overview of the ROS damage and its role in pathogenesis	6
Figure 1.3 Facilitated reaction path for AR and H ₂ O ₂ yielding fluorescent resorufin.....	12
Figure 1.4 Schematic presentation of mitochondrial ETC and site of inhibition	14
Figure 2.1 Schematic of the ventilation and perfusion of the isolated lung	19
Figure 2.2 PTI system.....	20
Figure 2.3 Photographs of the cuvette holder, cuvette, and probe.....	21
Figure 3.1 Resorufin standard curve.....	25
Figure 3.2 Equivalent amount of H ₂ O ₂ in recirculating perfusate	27
Figure 3.3 Amount of H ₂ O ₂ released from a representative lung.....	27
Figure 4.1 Inhibitor standard curves.....	31
Figure 4.2 Catalase standard curve	32
Figure 4.3 Rate of AR auto-oxidation to resorufin	34
Figure 4.4 Lung rates of H ₂ O ₂ release before and after inhibitor treatment	36
Figure 4.5 Lung rates of H ₂ O ₂ release before and after the addition of inhibitor solvents	37
Figure 4.6 Effect of hyperoxia on H ₂ O ₂ release.....	39
Figure 5.1 Schematic representation of mitochondrial ROS production and mitochondrial inhibitor sites.....	47
Figure 5.2 Arbitrary fluorescence measurement from recirculating lung samples with and without HRP.....	48

CHAPTER 1: INTRODUCTION, BACKGROUND, AND OBJECTIVE

1.1 Clinical Motivation

Acute lung injury (ALI) is a disease that occurs when the lung parenchyma, the site for the body's gas exchange, becomes inflamed. This inflammation leads to edema and hypoxemia due to impaired gas exchange, and can be accompanied by organ failure and eventually death due to multiple organ failure (Matthay, Ware, & Zimmerman, 2012).

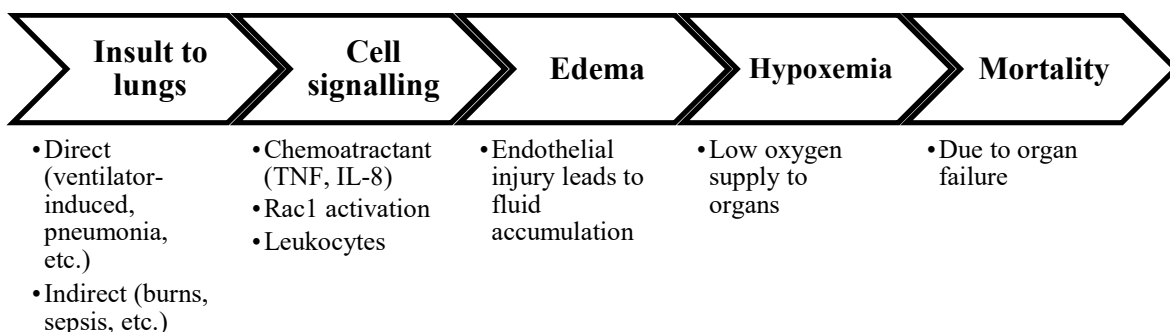


Figure 1.1: Progression of ALI/ARDS. The figure shows the progression of ALI/ARDS from insult to the lung to mortality/death.

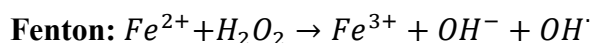
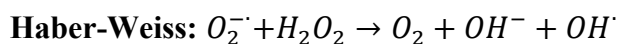
ALI can be caused by a direct (e.g. pneumonia and inhalation of harmful substances) or indirect insult (e.g. severe burns and sepsis) to the lungs, and remains a leading cause for admittance to intensive care units (Matthay et al., 2012). Acute Respiratory Distress Syndrome (ARDS) is the most severe form of ALI. The incidence of ARDS is ~200,000 new cases per year in the US with a mortality rate of >40% and over

\$5 billion in healthcare costs per year (Kumar et al., 2011). Current treatments of ALI/ARDS are mostly supportive. Thus, there is an urgent need for the development of novel therapies for ALI/ARDS.

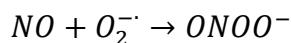
There is ample evidence that oxidative stress, defined as the imbalance between the rate of production of oxidants or reactive oxygen species (ROS) and the antioxidant mechanisms that scavenge ROS, plays a key role in the pathogenesis lung diseases including ALI/ARDS (Griffith et al., 2009; Mittal, Siddiqui, Tran, Reddy, & Malik, 2014). Thus, the ability to assess oxidative stress and to determine the major cellular sources of oxidative stress in intact functioning rat lungs is important for the identification of potential therapeutic targets, and for accelerating the screening, development, and testing of potential new therapies for their efficacy against ALI/ARDS.

1.2 Oxidative Stress: Reactive Oxygen Species (ROS), Antioxidant Mechanisms, and Cellular Sources of ROS

Some of the most damaging ROS include superoxide ($O_2^{\cdot-}$), hydroxyl radical (OH^{\cdot}), peroxynitrite ($ONOO^{\cdot-}$), and hydrogen peroxide (H_2O_2) (Mittal et al., 2014). For most cellular sources of ROS, $O_2^{\cdot-}$ is the primordial radical. However, $O_2^{\cdot-}$ is short lived (maintained at $<10^{-11}M$) and is quickly converted to secondary highly reactive intermediates such as H_2O_2 , OH^{\cdot} , and $ONOO^{\cdot-}$ through various reactions (Haffner, 2000). For instance, harmful OH^{\cdot} can be formed from $O_2^{\cdot-}$ with the Haber-Weiss reaction or from H_2O_2 with the Fenton reaction shown below:

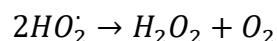


Peroxynitrite (ONOO^-) can form from the reaction of $\text{O}_2^{\cdot -}$ with another primordial radical, namely nitric oxide (NO) (Julio Turrens, 2003):



H_2O_2 can form from $\text{O}_2^{\cdot -}$ spontaneously via reaction with protons (which is facilitated by the relatively low pH in the intermembrane space of mitochondria) or via a reaction catalyzed by superoxide dismutase (SOD) (Mittal et al., 2014):

Spontaneous: $\text{O}_2^{\cdot -} + \text{H}^+ \rightarrow \text{HO}_2^{\cdot}$ (Hydroperoxyl radical)



SOD catalyzed: $2\text{O}_2^{\cdot -} + 2\text{H}^+ \xrightarrow{\text{SOD}} \text{H}_2\text{O}_2 + \text{O}_2$

Under physiological conditions, ROS play a role in many normal functions including cell signaling, regulation of vascular tone, and microbial defense (Klebanoff, 2005; Zhang & Gutterman, 2007a). However, ROS in excess can cause damage to healthy tissue. ROS-induced damage includes protein oxidation (changing the structure and affecting function), DNA damage (modifying bases and altering gene expression), and lipid peroxidation (affecting the function of the lipid by causing it to become more hydrophilic) (Haffner, 2000) and can even trigger apoptosis or programmed cell death (Audi et al., 2015).

Lipid peroxidation occurs readily in the membrane of cells due to the vulnerable nature and positive feedback reaction mechanisms of unsaturated lipids (found in the membrane) with ROS. Disrupting the lipid membrane is particularly important to healthy lung function because there are only two lipid membranes separating the alveolar air

space from the blood-filled capillaries. If this barrier is disrupted, edema, protein infiltration, inflammation, and eventually respiratory failure and hypoxemia can occur as seen in ALI/ARDS (Bayir & Kagan, 2008).

Cellular sources of ROS:

Sources of ROS in cells can be classified as mitochondrial or non-mitochondrial. For a given source, a specific inhibitor can be used to determine its contribution to the overall rate of ROS production by evaluating pre- and post-inhibitor rates (pharmacological approach) (Zhang & Gutterman, 2007a).

It is widely accepted that the electron transport chain (ETC), which is embedded in the mitochondrial inner membrane, is a major source of ROS (Chiang, Chuang, Liu, Lee, & Zhang, 2011; Mittal et al., 2014; Julie Turrens, Freeman, & Crapo, 1982; Julio Turrens, 2003). ETC components include NADH dehydrogenase (complex I), succinate dehydrogenase (complex II), ubiquinol-cytochrome *c* oxidoreductase (complex III), cytochrome *c* oxidase (complex IV), and ATP synthase (complex V). Complexes I and II reduce ubiquinone to ubiquinol which subsequently reduces complex III. Cytochrome *c* is also involved in the ETC by transferring electrons from complex III to complex IV and reduces O₂ to H₂O as an electron sink. This electron transfer facilitates pumping of H⁺ across the inner membrane at complexes I, III, and IV into the intermembrane space to create an electrochemical gradient. This gradient is then harnessed by complex V to form ATP from ADP.

The majority of electrons are delivered through the mitochondrial ETC productively during energy transduction, while a small fraction (~1-2%) of electrons leak

to O_2 prematurely, forming the free radical $O_2^{\cdot -}$ which can participate in further reactions to yield H_2O_2 or other more harmful forms of free radicals (Andreyev, Kushnareva, & Starkov, 2005; Muller, 2000).

While all complexes may leak electrons, previous studies have suggested that complex I and complex III are the main sources of mitochondrial ROS and produce a significant amount of $O_2^{\cdot -}$ under physiological and pathological conditions (Chen, Vazquez, Moghaddas, Hoppel, & Lesnefsky, 2003). However, other studies have suggested complex II, which connects the Krebs cycle to the ETC, as another major source of ROS and can influence the production of ROS at complexes I and III (Hoekstra & Bayley, 2013; Quinlan et al., 2012).

A study by Quinlan et al. asserts that complex II may contribute more to ROS production than previously thought, through both forward reactions with succinate and reverse reactions with ubiquinone (Quinlan et al., 2012). Complex II is made of four subunits and oxidizes succinate, from the Krebs cycle, to fumarate and reduces ubiquinone to ubiquinol and it is suggested that the flavin site of complex II can produce $O_2^{\cdot -}$ at high rates under *in vivo* conditions (Quinlan et al., 2012). Quinlan et al. showed a persistent rate of ROS production with complex I and III inhibited (by rotenone and myxothiazol, respectively) and *in vivo* concentrations of succinate (Quinlan et al., 2012). ROS production fully dispersed after the inhibition of complex II flavin site with malonate (Quinlan et al., 2012). Little is known about the contribution of complex II to ROS production in lungs under physiological or pathophysiological conditions.

Previous studies have suggested that the rate of mitochondrial ROS production via the ETC to be directly proportional to mitochondrial oxygen concentration and

inversely proportional to electron flow in the ETC, which slows when the mitochondrial complexes are impaired (Brueckl et al., 2006; Freeman, Topolosky, & Crapo, 1982; Kallet & Matthay, 2012). Potential pathways for mtROS-induced tissue injury are depicted in Figure 1.2 (Murphy, 2008a).

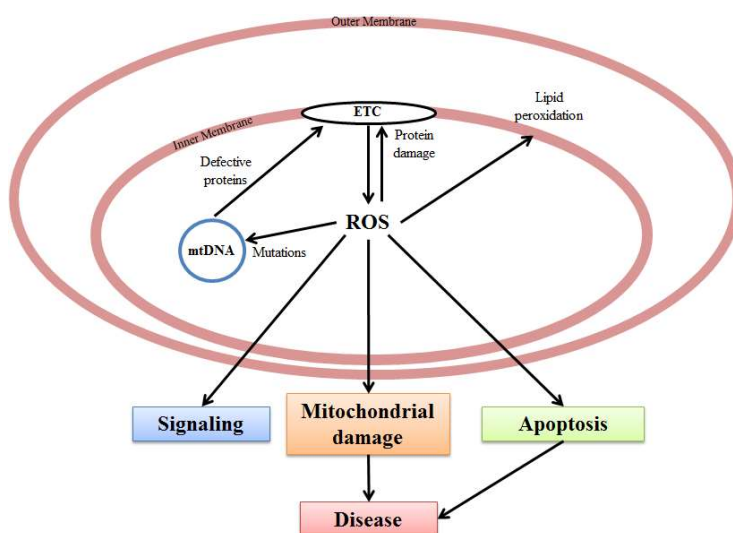
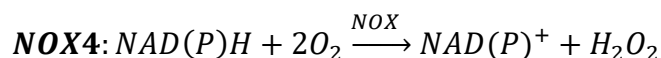
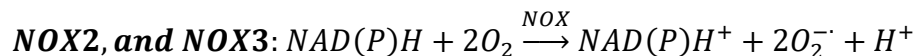


Figure 1.2: Overview of the ROS damage and its role in pathogenesis. ROS can damage proteins, membranes and DNA, which can impair mitochondrial function ATP and contribute to disease pathogenesis (reproduced from (Murphy, 2008a)).

Non-mitochondrial sources include NAD(P)H oxidase (NOX), xanthine oxidase, uncoupled endothelial nitric oxide synthase (eNOS), nitric oxide (NO) synthase, and arachidonic acid metabolizing enzymes including (e.g. cytochrome P-450) (Zhang & Gutterman, 2007a).

The NOX family consists of at least seven members (Cifuentes-Pagano, Meijles, & Pagano, 2014). NOX2, NOX3, and NOX4 are present in lung tissue (Griffith et al.,

2009). The overall reactions by which NOX2, and NOX3 generate $O_2^{\cdot -}$ and NOX4 generates H_2O_2 are:



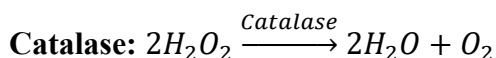
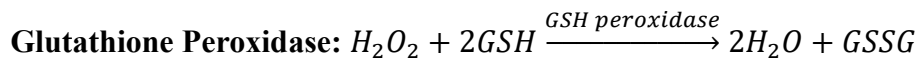
Griffith et al. showed that NOX2 is present in the pulmonary artery endothelial cells and in the macrophages and neutrophils present in the alveolar space and blood (Griffith et al., 2009). NOX3 is present in the endothelial cells (Griffith et al., 2009), and NOX4 is present in the pulmonary artery endothelial and smooth muscle cells, and in the myofibroblasts in the airways (Griffith et al., 2009).

NOX4 is a unique form of NOX because it produces ROS mainly (90%) as H_2O_2 rather than $O_2^{\cdot -}$ from molecular oxygen (Nisimoto, Diebold, Constantino-Gomes, & Lambeth, 2014). It is also important to note that NOX4 is regulated by oxygen level. Its Michaelis-Menten constant (K_m) for oxygen is relatively high (~18%) as compared for example to that for NOX2 (~2-3%), and hence may serve as an O_2 sensor in cells, with H_2O_2 serving as the signaling molecule (Nisimoto et al., 2014). This suggests that NOX4 may be an important source of ROS in high oxygen environments (hyperoxia) and hence may play an essential role in subsequent lung injury.

Cellular anti-oxidants:

In order to protect cells from the damage caused by ROS, cells have antioxidant defenses that scavenge the ROS before harmful reactions occur. Antioxidant defenses include enzymatic (e.g. SOD, glutathione peroxidase, and catalase, peroxiredoxins) and non-enzymatic (e.g. vitamins C and E, and glutathione) pathways (Haffner, 2000). For

example, H_2O_2 can be reduced to harmless water and oxygen molecules by peroxidases (e.g. glutathione peroxidase) and catalase:



Where GSH is glutathione and GSSG is the glutathione disulfide (oxidized form of GSH).

Within mitochondria, antioxidant defenses protect mitochondrial DNA (which encodes 13 proteins for the ETC (Kühlbrandt, 2015)), ETC complex proteins, and membrane integrity. The specific form of SOD with manganese in the active site (MnSOD) is found within the mitochondrial matrix and yields a less harmful H_2O_2 molecule from $O_2^{\cdot -}$ in the reaction shown previously. MnSOD present in mitochondria is sufficient for scavenging most $O_2^{\cdot -}$ directed into the matrix from the respiratory chain and the resulting uncharged H_2O_2 may pass through the membrane for further detoxification (Haffner, 2000).

In the cytoplasm, a copper zinc SOD is present to perform a similar detoxifying function as MnSOD for the $O_2^{\cdot -}$ directed towards the intermembrane space (i.e. Q_0 center of complex III). Another process that may occur in the intermembrane space of mitochondria is cytochrome c reduction by $O_2^{\cdot -}$ (concomitantly oxidized to harmless O_2) which then contributes to the energy pathway required for the complex IV H^+ pump (Julio Turrens, 2003).

Oxidative stress occurs when the scavenging rate of antioxidants is overwhelmed by an enhanced rate of ROS production, and as a result oxidant damage to cells increases and causes cellular injury and death.

Using mostly *in vitro* assays, including lung tissue homogenates, isolated mitochondrial, and cultured cells, previous studies have shown that the mitochondrial ETC produces the majority of cellular ROS (Zhang & Gutterman, 2007a) in various animal models of ALI, including hyperoxia- and lipopolysaccharide-induced ALI (Intae Lee, Dodia, Chatterjee, Feinstein, & Fisher, 2014). Although these reduced systems are important, particularly because of the range of manipulations, variable control, and detail of study that can be achieved, they cannot reproduce the multicellular environment and behavior of an intact, functioning lung under physiological and pathophysiological conditions. Thus, tools for evaluating ROS production in intact functioning lungs are necessary to allow further understanding of the role of oxidative stress in the pathogenesis of acute and chronic lung diseases including ALI/ARDS, and for identifying the main sources of ROS that contribute to this oxidative stress.

1.3 Methods for Measuring Cellular Rate of ROS Production

ROS can be measured optically with the use of specific fluorescent probes. Optical fluorescence imaging relies on the excitable nature (in the visible light spectrum) of certain fluorophores (fluorescent probes). These fluorophores absorb energy at a certain wavelength of light (excitation) and give off light energy at a lower energy and higher wavelength while returning to ground state (emission). There are two categories of optical imaging fluorophores, endogenous (produced by the cell such as NADH and FAD) and exogenous (introduced to the system such as Amplex Red). Furthermore,

exogenous fluorophores could be intracellular (able to cross the cell membrane) or extracellular (unable to cross the cell membrane).

Previous studies have mostly used fluorescent probes that are able to cross the cell membrane such as 2',7'-dichlorodihydrofluorescein diacetate (DCF) for general ROS measurement (Brueckl et al., 2006; Kalyanaramana, Balaraman Darley-Usmarb et al., 2013; Paddenberg et al., 2003) or hydroethidine (HE) for measuring $O_2^{\cdot-}$ production (Chatterjee, Chapman, & Fisher, 2008; Li et al., 2003). However, DCF can be problematic because the conversion of DCF after its reaction with ROS is irreversible and the converted form is not cell-permeable and hence may remain in the cell, potentially interfering with cellular function (Brueckl et al., 2006). Moreover, DCF can interact with many types of ROS, including hydroxyl radicals, H_2O_2 , and nitrite (NO_2^{\cdot}) (Kalyanaramana, Balaraman Darley-Usmarb et al., 2013), and hence the measured signal is not specific (Brueckl et al., 2006; Intae Lee et al., 2014).

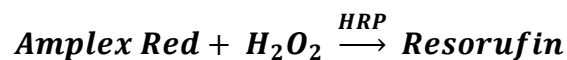
HE also has disadvantages as a specific probe for $O_2^{\cdot-}$, which is inherently difficult to measure in physiologic systems because the half-life of free $O_2^{\cdot-}$ in cells is relatively short and it does not diffuse through membranes due to its negative charge (Haffner, 2000). Measuring the transient $O_2^{\cdot-}$ radical makes interpretation of results difficult and may not capture the true physiologic status. In addition, HE binds to DNA after reacting with $O_2^{\cdot-}$ which can disrupt cellular function (Brueckl et al., 2006).

Brueckl et al. used DCF and HE to detect endothelial ROS production in isolated perfused rat lungs (Brueckl et al., 2006). For this study, fluorescence microscopy was used to image the pulmonary capillary endothelial cells and the intensity from images was then used to assess rates and sources of endothelial ROS production. In addition,

they show an enhanced rate of ROS production shortly following exposure to hyperoxia and a reduced rate of ROS production in the presence of the complex I inhibitor rotenone.

Weissmann et al. developed an approach for measuring ROS production in isolated, perfused rabbit and mouse lungs using electron spin resonance spectroscopy (ESR) with the spin probe 1-hydroxy-3-carboxy-2,2,5,5-tetramethylpyrrolidine (CPH) (Weissmann et al., 2005). CPH is cell permeable non-specific ROS scavenger that is oxidized by ROS to a stable nitroxyl CP radical which can be detected using ESR. Spin probes such as CPH are used at relatively high concentrations (mM range) and can accumulate in the cell and hence, could interfere with cellular functions. Furthermore, they are sensitive to transition metals that are found in perfusate. Hence, perfusate needs to be incubated with a chelating compound (deferoxamine or DTPA) overnight to minimize this effect (Dikalov & Harrison, 2014; Weissmann et al., 2005).

Unlike $O_2^{\cdot -}$, H_2O_2 has a much longer half-life, is relatively stable, and can readily diffuse across cellular membranes. Therefore, it is a more reliable ROS to measure and a more robust index of oxidative stress (Bienert, Schjoerring, & Jahn, 2006). Amplex Red (AR) is an extracellular fluorescent probe which is oxidized to highly fluorescent resorufin (excitation and emission wavelengths of 545 nm and 610 nm, respectively) in the presence of H_2O_2 and horseradish peroxidase (HRP) (Rhee, Chang, Jeong, & Kang, 2010).



AR has many advantages, including its minimal interaction with cellular functions, its sensitivity and specificity to H_2O_2 , and its reduced background fluorescence in comparison to other optical ROS probes (Brueckl et al., 2006; Chen et al., 2003; Zhou,

Diwu, Panchuk-Voloshina, & Haugland, 1997). Furthermore, since AR does not enter the cells, the rate of resorufin formation is then a measure of the net rate of H_2O_2 produced by the lung, which could arise from several sources within the lung tissue, and is influenced by the activities of various cellular anti-oxidants. Because AR is a measure of the ROS that have overwhelmed intracellular antioxidant defense and leaked to the extracellular space, then the rate of resorufin formation and hence rate of H_2O_2 released could be considered an index of the oxidative stress experienced by the lungs under a given condition.

1.4 Considerations for H_2O_2 Measurement with AR

For proper use of AR for H_2O_2 measurement, one needs to be aware of its limitations and potential sources of error. For instance, a previous study showed that in the presence of ascorbate, AR radical can convert back to AR without producing resorufin (Rodrigues & Gomes, 2010). The reaction is shown below in Figure 1.3 (Rodrigues & Gomes, 2010):

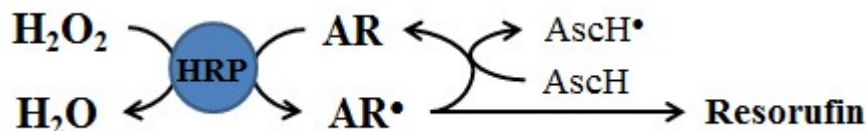


Figure 1.3: Facilitated reaction path for AR and H_2O_2 yielding fluorescent resorufin. There is a period in which the AR radical form can react with ascorbate ($AscH$) produced in the lung which will prevent resorufin formation. This interference can be prevented with the use of ascorbate oxidase.

Ascorbate is a protein released from rat lungs at a rate of 4.8-6.4 nanomol per minute (Audi et al., 2001). The reaction of ascorbate with AR radical begins to reduce the resorufin signal at a concentration of $\sim 1\mu\text{M}$ (Rodrigues & Gomes, 2010). Thus, ascorbate present after several minutes of circulation could cause a significant amount of interaction with AR radical and reduce the resorufin signal observed. Previous studies have not accounted for the effect of ascorbate released by the lungs on measured resorufin signal. The addition of ascorbate oxidase to the perfusate recirculating through the lungs is a way to minimize the impact of ascorbate released by the lungs on the measured resorufin signal (Audi et al., 2001).

Like most exogenous fluorophores, AR is sensitive to light and can photo-oxidize, leading to an erroneously high measurement (Zhao, Summers, & Mason, 2012). This issue can be minimized by performing experiments with minimal light exposure and using low energy red light when light is necessary (Zhao et al., 2012). Background increase in signal due to autoxidation over time during the experiment may be accounted for by performing experiments without an H_2O_2 source. The non- H_2O_2 induced signal increase may be removed from the signal measured with an H_2O_2 source (e.g. lung).

Other experimental considerations with the use of AR include a specified pH and linear range. A pH of 7-8 is required for accurate measurement (Instruments & Park, 2006). Also, resorufin fluorescent signal is linear up to $2.5\mu\text{M}$ and undergoes self-quenching at a concentration $>5\mu\text{M}$ (Instruments & Park, 2006).

1.5 Pharmacological Approach for Determining the Sources of Cellular ROS

To determine the contributions of various cellular ROS sources to the measured resorufin signal, a pharmacological approach can be used in which the effects of inhibitors on the rate of resorufin formation are determined. The inhibitors (Table 1.1) include mitochondrial (e.g. potassium cyanide, antimycin A, rotenone, and thenoyltrifluoroacetone) and NOX (e.g. apocynin, dihydroethylenediamine iodide (DHE)). Figure 1.4 shows the path of electrons in the respiratory chain and targets of various inhibitors. In the presence of rotenone, complex I will no longer oxidize NADH or reduce coenzyme Q. However, complex II will continue to reduce coenzyme Q for Complex III. Therefore, a measured change in the rate of ROS production (rate of resorufin formation) in the presence of rotenone can be attributed to complex I. The targets for other mitochondrial inhibitors are shown in Figure 1.4.

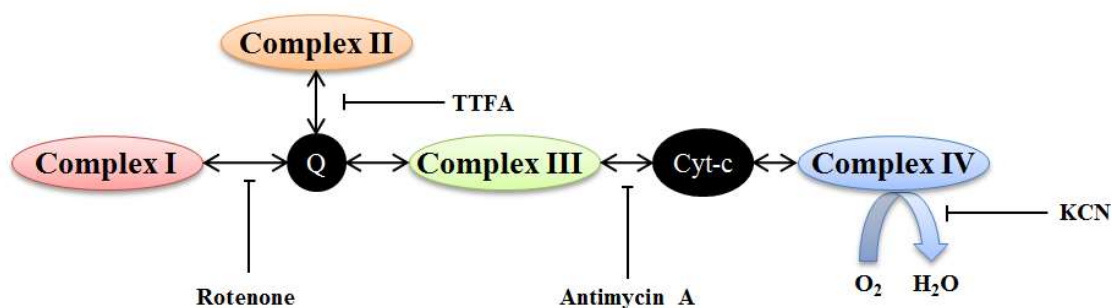


Figure 1.4: Schematic presentation of mitochondrial ETC and site of inhibition. The electron carriers are arranged spatially in the order of their increasing redox potential and organized into four complexes. The inhibited locations for rotenone, TFA, and Antimycin A, and KCN are shown.

Table 1.1: Mitochondrial ETC complex inhibitors and their targets. Each may have different effects on mitochondrial ROS production depending on the state, environment, and condition of the mitochondria.

Effects of Mitochondrial inhibitors	
Rotenone	<ul style="list-style-type: none"> - Complex I inhibitor - Inhibits the transfer of electrons from the iron-sulfur center in Complex I (Li et al., 2003) - Blocks transfer of electrons from NADH to coenzyme Q - Shown to reduce or have no effect on ROS production in conflicting studies (Campian, Qian, Gao, & Eaton, 2004; Chen et al., 2003) - Isolated mitochondria show an increase in ROS production and decreased ATP production (Li et al., 2003) - Sheep pulmonary microvascular endothelial cells exposed to hyperoxia (100% O₂ for 30 min) decrease ROS production when exposed to rotenone (Sanders et al., 1993)
Thenoyltrifluoroacetone (TTFA)	<ul style="list-style-type: none"> - Complex II inhibitor - Reduces the Q site of complex II (Quinlan et al., 2012)
Antimycin A	<ul style="list-style-type: none"> - Complex III inhibitor (Q_i) - Blocks the flow of electrons from semiquinone to ubiquinone via cytochrome b in the Q-cycle of complex III (Huang, Cobessia, Tung, & Berry, 2005) - Inhibits the ETC pathway and prevents transfer of electrons from coenzyme Q to cytochrome c (Huang et al., 2005),(Woo, Yong, Suh, & Sung, 2007) - Increased ROS production in isolated mitochondria (Chen et al., 2003)
Myxothiazol	<ul style="list-style-type: none"> - Complex III inhibitor (Q_o) - Decreased ROS production (Zhang & Gutterman, 2007b) - Can inhibit other components of the mitochondrial respiratory chain at high concentrations (Zhang & Gutterman, 2007b)
Cyanide	<ul style="list-style-type: none"> - Complex IV inhibitor - Affinity to heme iron within cytochrome oxidase prevents transfer of electrons from cytochrome c to oxygen
Azide	<ul style="list-style-type: none"> - Complex IV inhibitor - Increased ROS production in isolated mitochondria (Chen et al., 2003)
Oligomycin	<ul style="list-style-type: none"> - Blocks ATP synthase - Inhibits ATP synthase and thereby hyperpolarize mitochondrial membrane potential
DNP (2,4 dinitrophenol)	<ul style="list-style-type: none"> - Uncoupler - Diffuses across the inner mitochondrial membrane and carries protons across the membrane (protonophore) - Decreases proton gradient by allowing protons to reenter the mitochondrial matrix - Decreases mitochondrial efficiency (i.e. increases the number of protons needed to pump to produce one ATP molecule)

Diphenyleneiodonium chloride (DPI) can be used to inhibit NOX and determine its contribution to the signal measured using AR. It is worth noting that DPI is a nonspecific inhibitor and has been suggested to have cytotoxic effects at concentrations greater than 10 μM (Hirano et al., 2015).

AR was used to measure the rate of H_2O_2 release from isolated perfused mouse lungs under control conditions, ischemic conditions (Song, Al-Mehdi, & Fisher, 2001), and lipopolysaccharide (LPS) treatment (Intae Lee et al., 2014). In those studies, the sources of ROS under normoxic conditions were not identified, although Lee et al. found that the increase in the rate of H_2O_2 release under LPS conditions was attributed to NOX (Intae Lee et al., 2014). The changes seen following ischemia were described by Song et al. in terms of increased resorufin signal, but there was not a pharmacological approach to determine the specific mitochondrial and non-mitochondrial contributions (Song et al., 2001). However, the increase in ROS production was correlated with an increase in Ca^{2+} which can subsequently cause NOX activation.

1.6 Objective

AR has been used previously to measure the rate of H_2O_2 production mostly in *in vitro* assays including isolated mitochondria, cultured cells, and tissue homogenates (Freeman et al., 1982; Murphy, 2008b). Few studies have used AR to measure the rate of H_2O_2 production in intact organs, including isolated perfused mouse lungs (Chatterjee et al., 2011). Furthermore, previous studies in organs did not take into consideration the potential interactions between AR and compounds released from lungs, including ascorbate, or auto-oxidation (Intae Lee et al., 2014; Zhou et al., 1997). To the best of our knowledge, AR has never been used to measure the rate of H_2O_2 production in the

isolated perfused rat lung. *Thus, the main objective of this thesis was to develop a robust protocol for using AR to measure the rate of H_2O_2 production in isolated perfused rat lungs and to determine the cellular sources of the measured H_2O_2 .*

CHAPTER 2: EXPERIMENTAL METHODS

2.1 Materials

Amplex Red and all other reagents used in experiments were purchased from Sigma-Aldrich (St. Louis, MO).

2.2 Isolated, Perfused Rat Lung Preparation

All animal protocols described below have been approved by the Institutional Animal Care and Use Committees of the Veterans Affairs Medical Center and Marquette University (Milwaukee, WI).

Adult male adult Sprague-Dawley rats ($349 \pm 4\text{g}$ (SE), $n = 37$) were used for this study. Each rat was anesthetized with sodium pentobarbital (40-50 mg/kg) and a midline sternotomy was performed (see Appendix A.2). Heparin was injected into the right ventricle and cannulas were placed in the pulmonary artery via the right ventricle, in the pulmonary vein via the left ventricle, and in the trachea. The lungs were then removed and attached to the ventilation-perfusion system using the pulmonary artery and trachea cannulas (Figure 2.1). The system included a roller pump (Masterflex LS, model: 7518-00) and a rodent ventilator (Harvard Rodent Ventilator). Pressure transducers were used to monitor the pressure in the airway and the pulmonary artery.

The perfusate used was Krebs-Ringer bicarbonate solution containing (in mM) 4.7 KCl, 2.51 CaCl₂, 1.19 MgSO₄, 2.5 KH₂PO₄, 118 NaCl, 25 NaHCO₃, 5.5 glucose, with 3% bovine serum albumin at 7.4 pH (Sepehr et al., 2013).

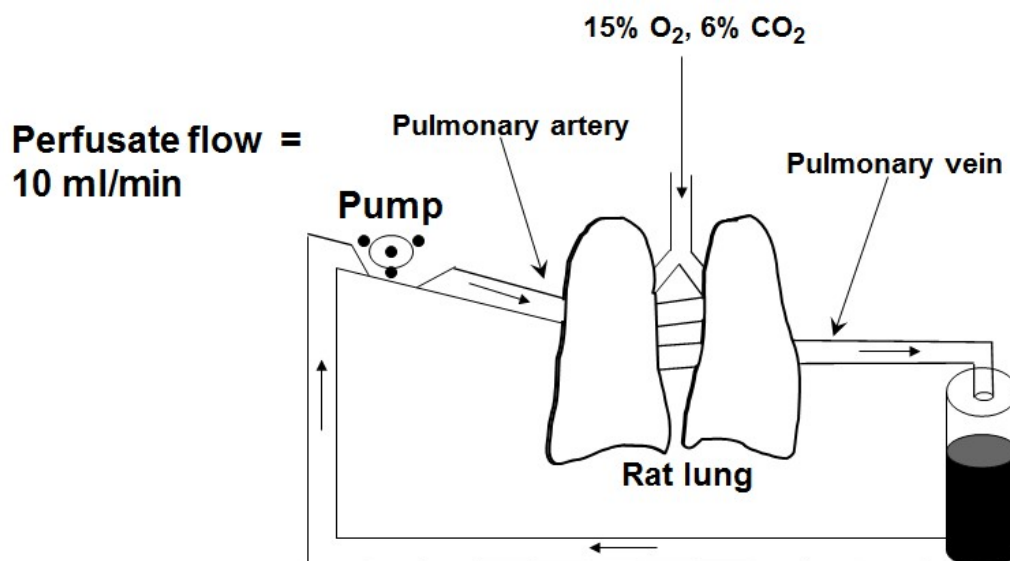


Figure 2.1: Schematic of the ventilation and perfusion of the isolated lung.

2.3 Optical Fluorescent Imaging System

The PTI Fluorometer: RatioMaster fluorescence imaging system (Photon Technology International, HORIBA Scientific) used for this study (Figure 2.2) is housed in the Pulmonary Research Laboratory at the Zablocki VA hospital. This state-of-the-art system provides temporal information of up to 1000 frames/second in real time. The system was used to quantify the rate of conversion of AR to resorufin in samples of perfusate recirculated through isolated perfused lungs as a measure of the lung's rate of H_2O_2 production. The monochromator was set to an excitation wavelength of 545 nm (xenon bulb light source), and the wavelength of the emission filter is 610 ± 15 nm (Chroma Technology Corporation, Bellows Falls, Vermont). The system is operated and controlled using custom software (FelixGX-4.3.2010).



Figure 2.2: PTI system.

2.4 Experimental Protocols

Once the lung was connected to the ventilation-perfusion system, it was perfused (single pass at a flow rate of 10 ml/min) with described Krebs-Ringer bicarbonate perfusate until it was clear of blood. After that, the perfusion was changed from single pass to recirculation (see Figure 2.1). The total volume of the system was 25 ml, 5 ml of which were the perfusion system tubing and the lung vasculature (leaving 19 ml in the reservoir). Both airway and arterial pressures were continuously measured and recorded.

Once the lung was clear of blood, the flow was stopped and the perfusate in the reservoir emptied and replaced with 19 ml of perfusate with 5 U/ml HRP, 25 μ M AR, and 1 U/ml ascorbate oxidase (AO). The flow (10 ml/min) was then restarted (time 0 min) and two 1-ml reservoir samples were collected at times 1 min, 6 min, and 11 min. The

sample collected at 1 min provided the background signal, whereas the samples at 6 min and 11 min provided the baseline rate of lung H_2O_2 production as described in the Data Analysis chapter. Immediately after each sample was collected from the reservoir, it was centrifuged for 1 min (13,000 g, 4°C) to remove any cellular components and debris. The sample supernatant was then transferred into a plastic cuvette and its 610 emission signal was measured using a fiber optic probe connected to a custom made cuvette holder (Figure 2.3). Soon after the signal was acquired, the sample was added back to the reservoir.

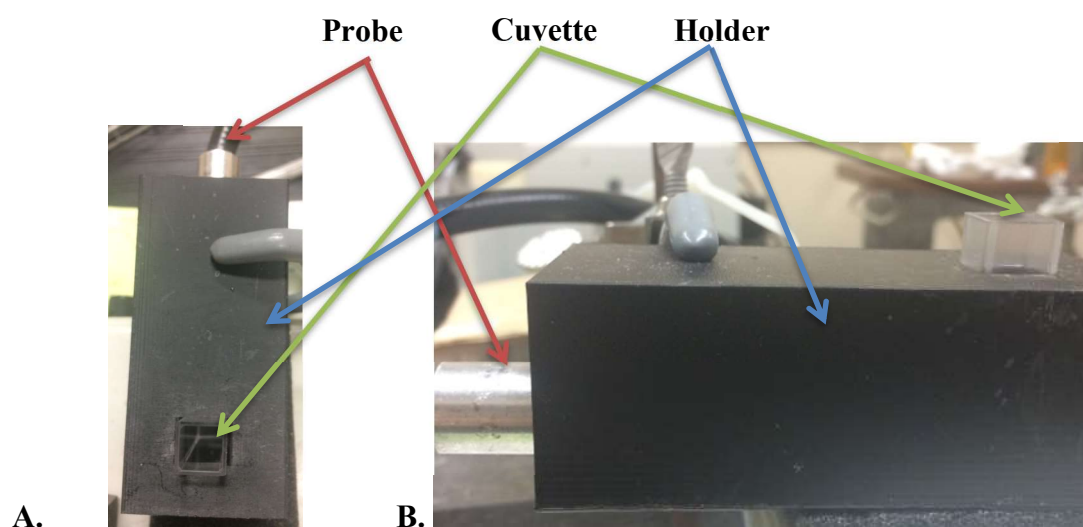


Figure 2.3: Photographs of the cuvette holder, cuvette, and probe from a top-view (A) and side-view (B).

To determine the contribution of a given cellular source to the measured baseline rate, an inhibitor was added to the recirculating perfusate at time 11 min (soon after the sample at 11 min was collected). This was followed by collecting two 1-ml reservoir

samples at times 16 min, 21 min, and 26 min. The measured signals from those samples were then used to determine the effect of the inhibitor on the baseline lung rate of H_2O_2 release as described in the Data Analysis chapter. Each sample was treated in the same manner as described above and its emission signal was then measured, after which it was added back to the reservoir. Another inhibitor could be added to the reservoir after the sample at 26 min was collected and additional samples collected every 5 min for the subsequent 15 minutes. It is important to note that this protocol is limited by the linear range of the resorufin signal. The entire protocol was carried out in a dark room (with red light) to minimize auto-oxidation of AR. Once all samples' emission signals were recorded, the information was then exported to a text file for offline analysis.

To determine the effect of complex I on the measured rate, the above protocol was carried out before and after the addition of rotenone ($40 \mu\text{M}$) to the recirculation perfusate (Barrientos & Moraes, 1999). To achieve this concentration, $10 \mu\text{l}$ of the stock (100 mM in DMSO) was added. For the effect of complex II on the measured rate, the above protocol was carried out before and after the addition of TTFA ($20 \mu\text{M}$) to the recirculation perfusate (Paddenberg et al., 2003). To achieve this concentration, $12.5 \mu\text{l}$ of the stock (40 mM in DMSO) was added. For determination of the effect of complex III on the measured rate, the above protocol was carried out before and after the addition of Antimycin A ($3.76 \mu\text{M}$) to the recirculation perfusate (Goncalves, Quinlan, Perevoshchikova, Hey-Mogensen, & Brand, 2015). To achieve this concentration, $5 \mu\text{l}$ of the stock (18.8 mM in 95% ethanol) was added. In order to determine complex IV's effect on the measured rate, the above protocol was carried out before and after the addition of KCN (2 mM) (Sepehr et al., 2013) to the recirculating perfusate. This was

achieved by adding 50 μ l of the inhibitor stock (1 M KCN in 0.5 M KH₂PO₄). Finally, the effect of NOX on the measured rate was determined by repeating the above protocol before and after the addition of DPI (5 μ M) to the recirculating perfusate (Koziel, Sobieraj, & Jarmuszkiewicz, 2015). This required the addition of 7.9 μ l of the inhibitor stock (15.8 mM in DMSO).

For each condition, the number of lungs studied (4-6) was based on results from previous studies by Fisher et al. in which they measured the rate of H₂O₂ release from isolated perfused mouse lungs using Amplex Red (Intae Lee et al., 2014).

To determine the impact of the inhibitor vehicles (DMSO, phosphate buffer, or 95% ethanol) alone on the lung rate of H₂O₂ release, for each of the vehicles the above protocol was repeated in a different group of lungs with the vehicle only (instead of inhibitor + vehicle) added at time 11 min to the recirculating perfusate.

At the end of the above protocol, the lungs were removed from the system and the lungs wet weight was measured and recorded. The lungs were then dried (2 days in an oven at 60°C) and their dry weight was then measured and recorded. The dry lung weight was used to normalize the measured rate of H₂O₂ production as described in the Data Analysis chapter.

2.4.1 Lung-Independent Rate of AR Conversion to Resorufin

To determine the portion of the measured resorufin signal using the above protocol that was due to auto-oxidation, the above protocol was repeated without the lung connected the ventilation-perfusion system. The measured rate of resorufin formation was attributed to auto-oxidation and hence was subtracted from the overall rate as described in the Data Analysis Chapter.

2.4.2 Standard Curve

For each day of experiments, a standard curve was obtained as described below and used to convert resorufin signal to H_2O_2 concentration in lung recirculation perfusate. Four tubes, each containing 4 ml of perfusate that included HRP and AR at the same concentrations as those used in the lung experimental protocol described above were prepared. A predetermined volume of 0.2 mM H_2O_2 was added to each of the four tubes for final H_2O_2 concentrations of 0 μM , 1 μM , 2 μM , and 3 μM in tubes 1, 2, 3 and 4, respectively. For each tube, a 2-ml sample was then treated the same way as the samples collected from the reservoir with the lung collected to the ventilation-perfusion system. Thus, each sample was centrifuged for 1 min (13,000 g, 4°C), after which its 610 nm emission signal was measured as described above. Once all samples emission signals were recorded, the information was then exported to a text file for offline analysis.

For a given inhibitor, the above standard curve was repeated with the inhibitor added to the samples prior to the addition of H_2O_2 to ensure that neither inhibitor nor its vehicle interfered with the resorufin signal.

CHAPTER 3: DATA ANALYSIS

Data analysis was performed in *Excel* using text files exported from PTI's Felix software.

3.1 Standard Curve

For each standard concentration, the raw intensity, in counts per second, was determined from the average of the samples taken over a period of 5 seconds. The measured intensities were then plotted against the known H_2O_2 concentrations. An example of a standard curve is shown in Figure 3.1. The slope of the standard curve was then used to convert resorufin intensity in a given reservoir sample (without or with lungs connected to the ventilation-perfusion system) collected at a given sampling time to concentration of H_2O_2 in the recirculating perfusate at that time.

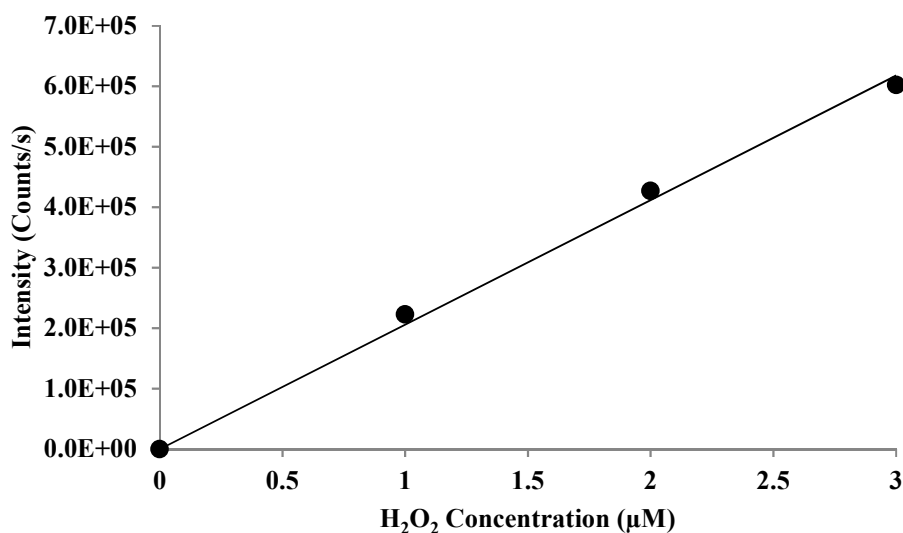


Figure 3.1: Resorufin standard curve. Standard curve relating fluorescent emission signal to H_2O_2 concentration.

Standard curves were obtained in the presence of each inhibitor to assess its effect on the measured signal.

3.2 Lung Data

For each reservoir sample at a given sampling time, the raw intensity, in counts per second, was determined from the average (over a period of 5 seconds) of the samples taken. The intensity of the sample collected at time 1 min was considered background intensity and was subtracted from the intensities of all subsequent samples. The slope of the standard curve for that day of experiments was then used to convert the intensity to H₂O₂ concentration in the recirculating perfusate (with or without lung attached to the ventilation-perfusion system) in the reservoir at the time the sample is collected. The amount of H₂O₂ (in nanomol) in the 25-ml system at the time the sample was then obtained as the product of the H₂O₂ concentration and volume of perfusate in perfusion system (25 ml). The result of this analysis was the amount of H₂O₂ in the system as a function of recirculation time with and without the lung attached to the ventilation-perfusion system. Using linear regression, the rates of H₂O₂ generation without and with the lung attached to the perfusion system were obtained as exemplified in Figure 3.2.

Please note that the rate of H₂O₂ generation without the lungs attached to the perfusion system was determined using a separate groups of experiments (n = 3). For a given lung, the average rate of apparent H₂O₂ generation (nmol/min) from those three experiments (0.43 ± 0.02 (SE) nmol/min) was then subtracted from the rate of H₂O₂ generation with the lungs connected to the ventilation perfusion system. The difference is then reported as the lung rate of H₂O₂ release into the recirculation perfusate. To account for differences in rat body weights and hence lung weights, the measured rate of lung

H_2O_2 release was normalized to lung dry weight and expressed as nmol/min/g dry lung wt.

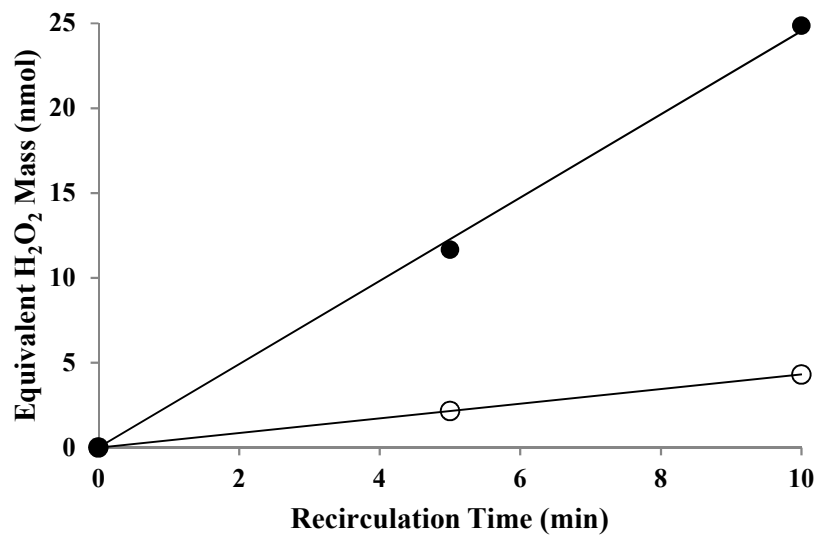


Figure 3.2: Equivalent amount of H_2O_2 in recirculating perfusate from the lung (●) and from the background auto-oxidation (○).

To account for differences in rat body weights and hence lung weights, the measured rate of lung H_2O_2 release was normalized to lung dry weight and expressed as nmol/min/g dry lung wt (3.3).

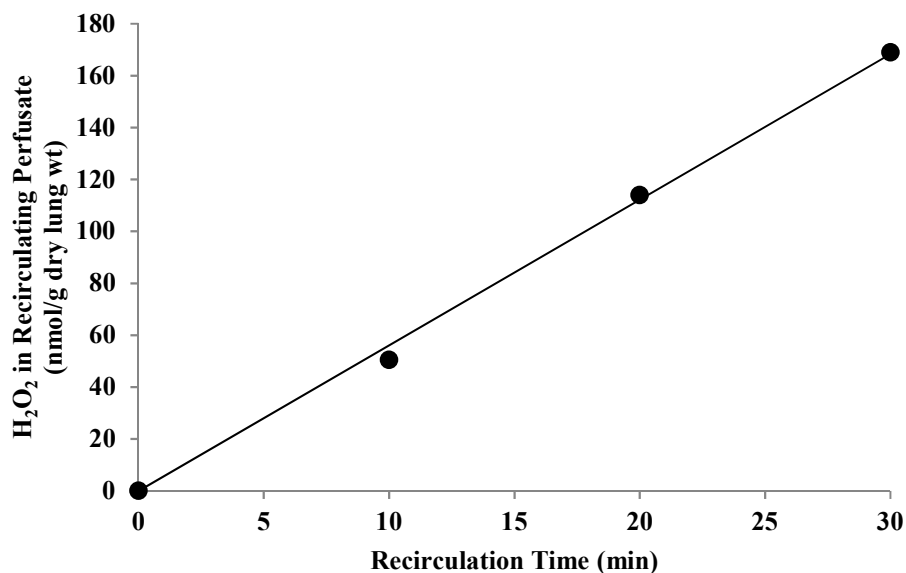


Figure 3.3: Amount of H₂O₂ released from a representative lung into the perfusate recirculating through the lungs as a function of recirculation time.

3.3 Statistical Analysis

Statistical analysis was completed on SigmaPlot software version 12.0 (Systat Software Inc., San Jose, CA.) using a paired *t*-test for compared two data sets collected from the same lung and unpaired *t*-test or ANOVA for comparison of more than two data sets. Statistical significance is specified as $p < 0.05$.

CHAPTER 4: RESULTS

4.1 Rats Body Weights, Lung Wet Weights, Dry Weights, and Wet-to-Dry Weight Ratios, and Pulmonary Artery Pressures

Table 4.1 shows rat body weights, lung wet and dry weights and wet-to-dry weights along with pulmonary artery pressures for each of the experimental conditions studied.

Table 4.1: Body weight, lung wet weight, dry lung weight, and wet-to-dry weight ratio for each of the experimental conditions.

Inhibitor/ Vehicle	Body weight (g)	Lung wet weight (g)	Lung dry weight (g)	Wet-to-dry weight ratio	Pulmonary Artery Pressure (mmHg)
+Ethanol	346 ± 9 (n = 3)	1.23 ± 0.05 (n = 3)	0.224 ± 0.004 (n = 3)	5.50 ± 0.16 (n = 3)	6.3 ± 0.3 (n = 3)
+ DMSO	339 ± 16 (n = 4)	1.39 ± 0.06 (n = 4)	0.232 ± 0.011 (n = 4)	5.65 ± 0.09 (n = 4)	6.2 ± 0.2 (n = 4)
+ KH ₂ PO ₄	350 ± 16 (n = 4)	1.33 ± 0.05 (n = 4)	0.238 ± 0.008 (n = 4)	5.60 ± 0.08 (n = 4)	6.3 ± 0.3 (n = 4)
+95% O ₂	350 ± 9 (n = 4)	1.26 ± 0.05 (n = 4)	0.228 ± 0.005 (n = 4)	5.51 ± 0.14 (n = 4)	6.6 ± 0.2 (n = 4)
+ROT	379 ± 8 (n = 4)	1.39 ± 0.03 (n = 4)	0.255 ± 0.013 (n = 4)	5.49 ± 0.33 (n = 4)	6.3 ± 0.4 (n = 4)
+TTFA	334 ± 11 (n = 6)	1.28 ± 0.06 (n = 6)	0.225 ± 0.008 (n = 6)	5.69 ± 0.31 (n = 6)	6.3 ± 0.3 (n = 6)
+AA	341 ± 19 (n = 4)	1.31 ± 0.06 (n = 4)	0.222 ± 0.005 (n = 4)	5.92 ± 0.24 (n = 4)	6.8 ± 0.3 (n = 4)
+KCN	350 ± 12 (n = 4)	1.24 ± 0.03 (n = 4)	0.225 ± 0.010 (n = 4)	5.51 ± 0.17 (n = 4)	6.0 ± 0.2 (n = 4)
+DPI	363 ± 11 (n = 4)	1.24 ± 0.04 (n = 4)	0.220 ± 0.009 (n = 4)	5.59 ± 0.07 (n = 4)	6.9 ± 0.3 (n = 4)

Values are mean \pm SE. Ethanol, dimethyl sulfoxide (DMSO), 0.5 M phosphate buffer (KH_2PO_4), rotenone (ROT), thenoyltrifluoroacetone (TTFA), antimycin A (AA), potassium cyanide (KCN), diphenyleneiodonium chloride (DPI).

ANOVA statistical analysis showed no difference in body weight ($p = 0.311$), lung wet weight ($p = 0.452$), lung dry weight ($p = 0.139$), wet-to-dry weight ratio ($p = 0.654$), or pulmonary artery pressure ($p = 0.385$) between the various experimental groups.

4.2 Resorufin Standard Curves Without and With Mitochondrial or NOX Inhibitors

Figure 4.1 shows standard curves without and with DPI (panel A), rotenone (panel B), TTFA (panel C), antimycin A (panel D), or potassium cyanide (panel E) added to the standard perfusate samples. These results show that only potassium cyanide (KCN) had a significant effect on the resorufin emission signal. KCN appears to quench the resorufin signal, with the slope of the standard curve scaled down by ~60%. This quenching effect was accounted for in the analysis of the resorufin signal measured in perfusate recirculating through the lungs in the presence of KCN.

For a given day, a standard curve was obtained under the same experimental conditions for that day and was used to convert resorufin signal to H_2O_2 concentration in the recirculating perfusate.

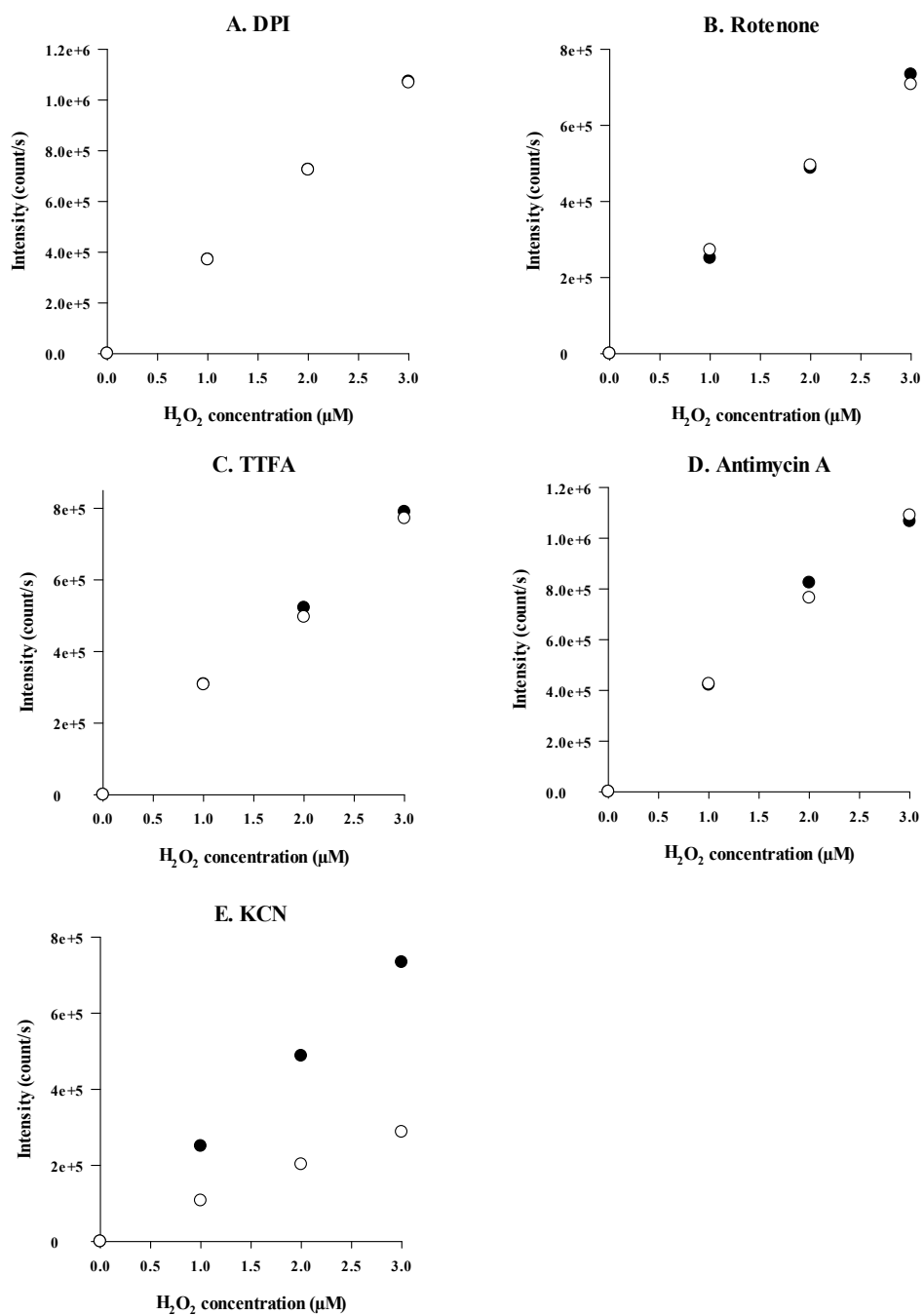


Figure 4.1: Inhibitor standard curves with (○) or without (●) 2,4 dinitrophenol (DPI, panel A), rotenone (ROT, Panel B), thenoyltrifluoroacetone (TTFA, Panel C), antimycin A (AA, Panel D), or potassium cyanide (KCN, Panel E).

Standard curve experiments with catalase were carried out to demonstrate the specificity of resorufin signal to H_2O_2 . Figure 4.2 shows that addition of catalase to the standard curve samples, followed by the addition of H_2O_2 , AR, and HRP, respectively, reduced the resorufin signal in the samples to zero, consistent with the ability of catalase to scavenge H_2O_2 and prevent its reaction with AR.

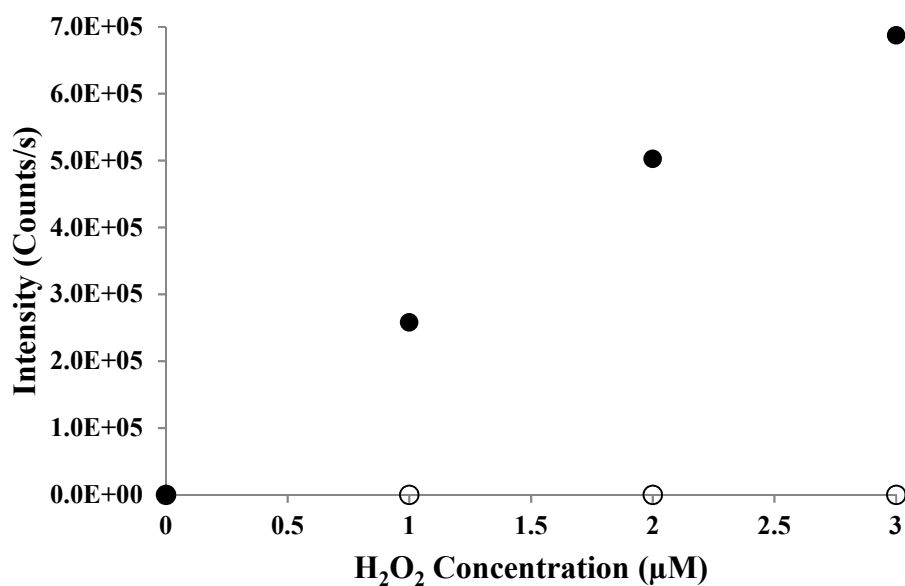


Figure 4.2: Catalase standard curve with (○) or without (●) catalase added to the samples.

4.3 Amplex Red Auto-Oxidation Rate

AR can auto-oxidize into resorufin in the presence of HRP. To estimate this auto-oxidation rate, AR and HRP were added to the reservoir of the ventilation-perfusion system without the lungs connected to the system and with the flow rate set at 10 ml/min. The rate of resorufin formation was measured using the same protocol as used with the lungs connected to the ventilation-perfusion system. Figure 4.3 shows the auto-oxidation rate of AR to resorufin, which was then converted to an “equivalent rate” of H₂O₂ formation using a standard curve. The rate was 0.43 ± 0.02 (SE, n = 3) nmol/min. The auto-oxidation rate of resorufin formation is ~6% of the rate of resorufin measured with the lungs added to the ventilation-perfusion system. For each experiment, this auto-oxidation rate was subtracted from the rate (nmol/min) estimated with the lungs connected the ventilation-perfusion system (Figure 4.3). The difference is then the rate (nmol/min) of H₂O₂ released by the lungs. For a given lung, this rate was then normalized to the lung’s dry weight to account for differences in lung weights. In what follows, the lung rate of H₂O₂ release is reported in units of nmol/min/g dry lung wt.

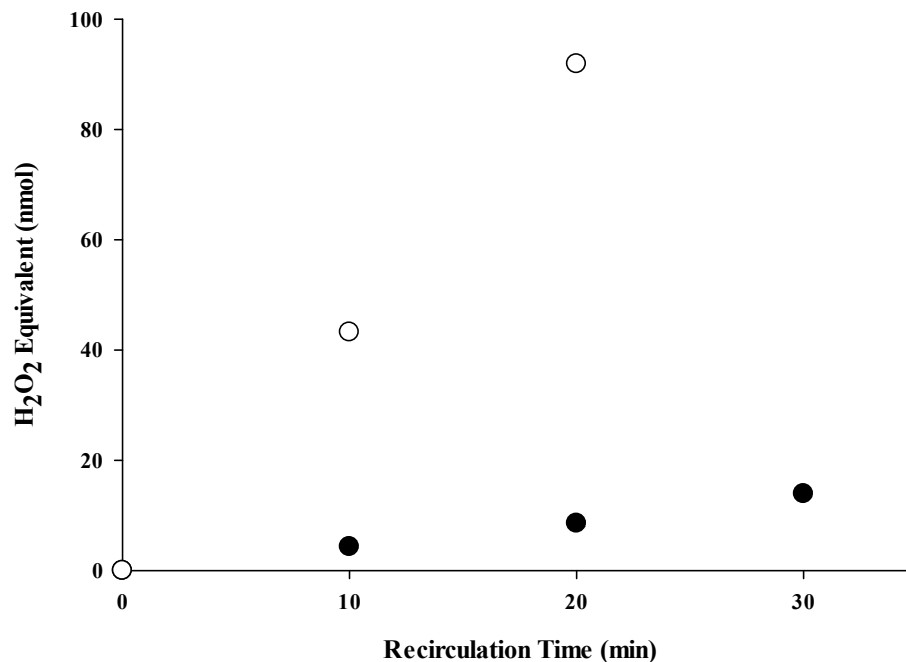


Figure 4.3: Rate of AR auto-oxidation to resorufin as a function of recirculation time following the addition of AR + HRP to the recirculating perfusate with (○) or without (●) the lung connected to the ventilation-perfusion system. For the data without the lungs connected to the ventilation-perfusion system, values are mean \pm SE, $N = 3$. The data with the lung connected to the ventilation-perfusion system was from a representative lung ($n = 1$).

4.4 Lung Rate of H₂O₂ Release and the Contributions of Mitochondria and NOX to this Rate

The lung rate of H₂O₂ release under normoxic ventilation conditions (15% O₂, 6% CO₂, balance N₂) was 8.32 ± 0.32 (SE, $N = 33$) nmol/min/g dry lung wt. Figure 4.4 shows that lung treatment with the mitochondrial complex II inhibitor (TTFA) decreased the lung rate of H₂O₂ release by ~76% (paired t -test, $p = 0.002$), whereas lung treatment with the NOX inhibitor DPI decreased the rate by ~23% (paired t -test, $p = 0.004$). Moreover, Figure 4.4 shows that lung treatment with the complex I inhibitor rotenone

(ROT) had a small (~13%), but significant (paired *t*-test, $p = 0.043$) effect on the lung rate of H₂O₂ release, whereas lung treatment with the complex III inhibitor antimycin A (AA) had no significant effect on this rate (paired *t*-test, $p = 0.315$). On the other hand, lung treatment with complex IV inhibitor potassium cyanide (KCN) increased the lung rate of H₂O₂ release by ~310% (paired *t*-test, $p = 0.004$).

These results suggest that in normoxic lungs most of the rate of H₂O₂ release, and hence ROS formation, is from the mitochondrial electron transport chain, and that the rates measured with and without DPI can be used to determine the mitochondrial and NOX contributions, respectively. Statistical analysis results show that the lung rates of H₂O₂ release under control conditions for the different experimental conditions (Figure 4.4) are not significantly different (ANOVA, $p = 0.387$).

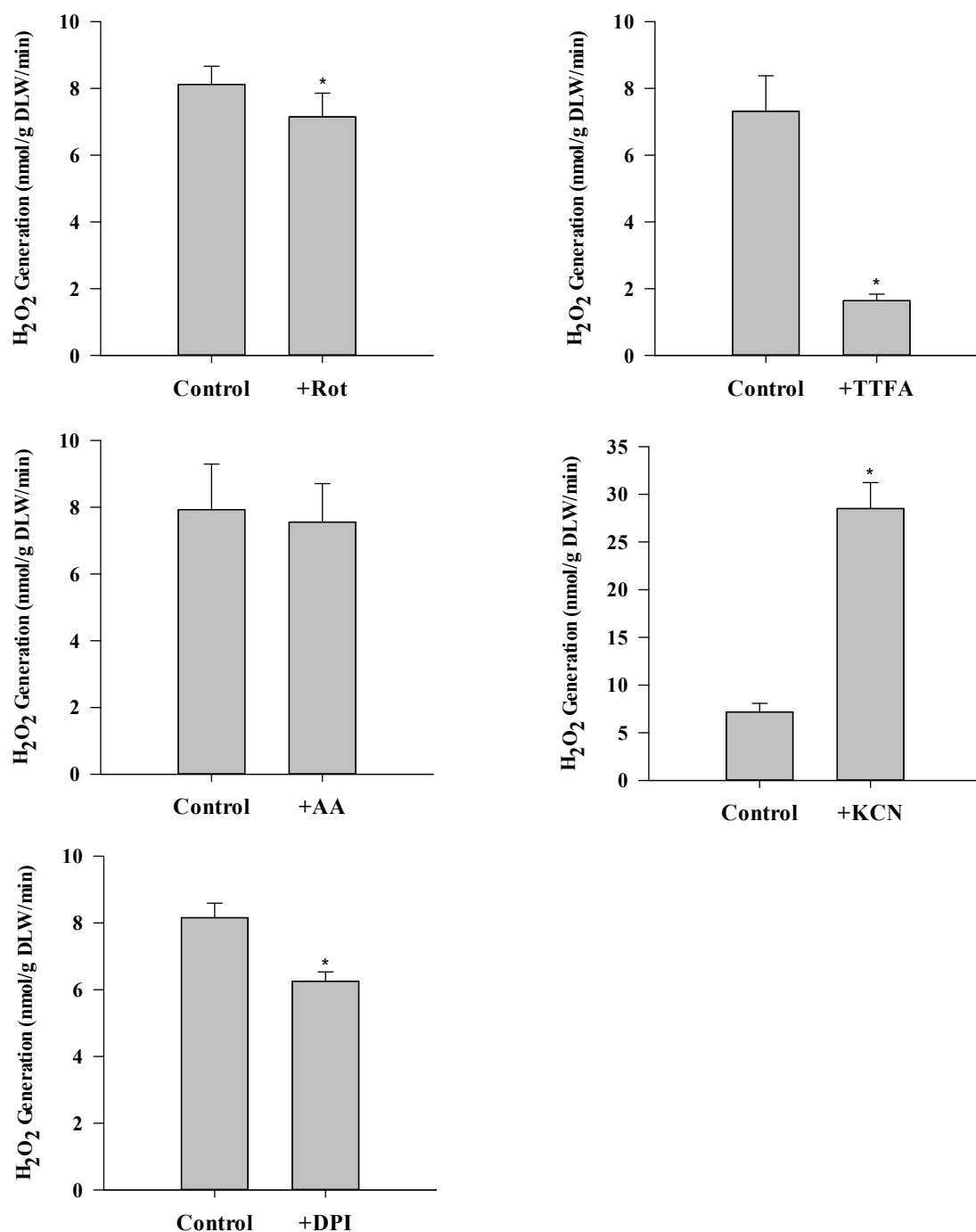


Figure 4.4: Lung rates of H₂O₂ release before and after inhibitor treatment with rotenone (ROT, panel A, n = 4), thenoyltrifluoroacetone (TTFA, panel B, n = 6), antimycin A (AA, panel C, n = 4), potassium cyanide (KCN, panel D, n = 4), or DPI (panel E, n = 4). Values are mean ± SE. * significantly different from the corresponding rate without any inhibitor, paired t-test (p < 0.05).

4.5 Effects of Mitochondrial/NOX Inhibitor Vehicles on Measured Rates of Lung H₂O₂ Release

For the inhibitors used, the vehicles were DMSO (for rotenone, TTFA, and DPI), phosphate buffer (for potassium cyanide), and 95% ethanol (for antimycin A).

Experiments were carried out to determine the effect of each of these vehicles on the measured rate of lung H₂O₂ release. Figure 4.5 shows that none of the vehicles had a significant effect (paired *t*-test, *p* = 0.431, 0.108, and 0.288 for DMSO, phosphate buffer, and ethanol, respectively) on the measured rate.

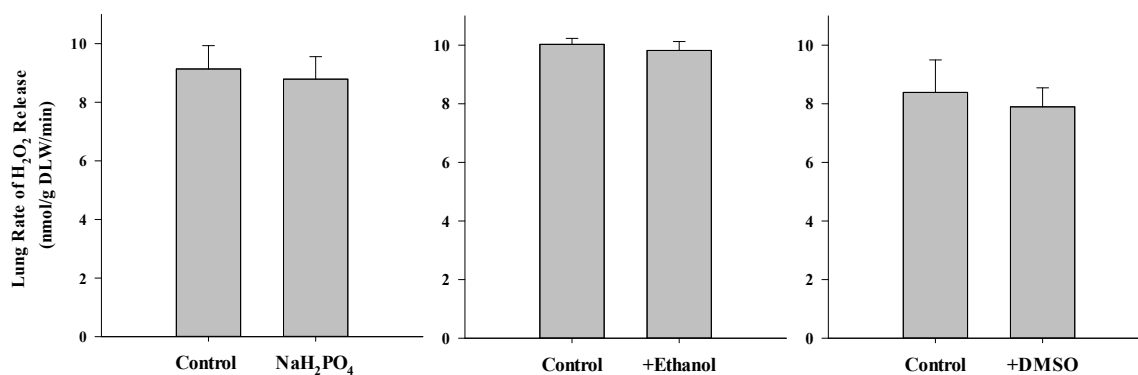


Figure 4.5: Lung rates of H₂O₂ release before and after the addition of inhibitor solvents 50μl of a 0.5 M KH₂PO₄ buffer (*n* = 4), 12.5μl DMSO (*n* = 4), or 5μl 95% ethanol (*n*=3) to the recirculating perfusate.

Statistical analysis results show the lung rates of H₂O₂ release under control conditions for the different experimental conditions (Figure 4.5) are not significantly different (ANOVA, *p* =0.601).

4.6 Effect of O₂ Level in Ventilation Gas on the Lung Rate of H₂O₂ Release

Previous studies have suggested that the lung rate of ROS formation is dependent on the level of oxygen (O₂) in the ventilation gas mixture (Brueckl et al., 2006; Nisimoto et al., 2014). This would be consistent with a role for oxidative stress in hyperoxia-induced lung injury (Freeman et al., 1982; Kinnula, Chang, Ho, & Crapo, 1992). To evaluate the effect of O₂ level on lung rate of ROS formation, for a group of lungs (n = 4) we evaluated the lung rate of H₂O₂ release following lung ventilation with either normoxic gas mixture (15% O₂, 6% CO₂, balance N₂) or hyperoxic gas mixture (95% O₂ + 5% CO₂). Figure 4.6 (Panel A) shows that the measured rate of H₂O₂ release at 95% O₂ (13.31 ± 0.58 (SE) nmol/min/g dry lung wt) was ~27% higher (paired *t*-test, *p*=0.026) than that measured at 15% O₂ (10.47 ± 0.68).

To begin to determine how much of this increase in the rate of lung H₂O₂ release at 95% O₂ is from mitochondrial sources and how much from NOX, for another group of lungs we measured the rate of H₂O₂ release in the presence of TTFA with the lungs ventilated first with normoxic gas mixture and then with hyperoxic gas mixture. The results in Figure 4.6 (Panel B) show that the rate of lung H₂O₂ release at 95% O₂ (4.96 ± 0.05 , n = 4) was 154% larger than the rate at 15% O₂ rate (1.95 ± 0.11); suggesting that most of the O₂-dependent increase in lung H₂O₂ release is non-mitochondrial. This result is consistent with the fact that NOX4 rate of ROS formation has a relatively large Michaelis-Menten constant ($K_m = \sim 18\%$) for O₂ (Nisimoto et al., 2014).

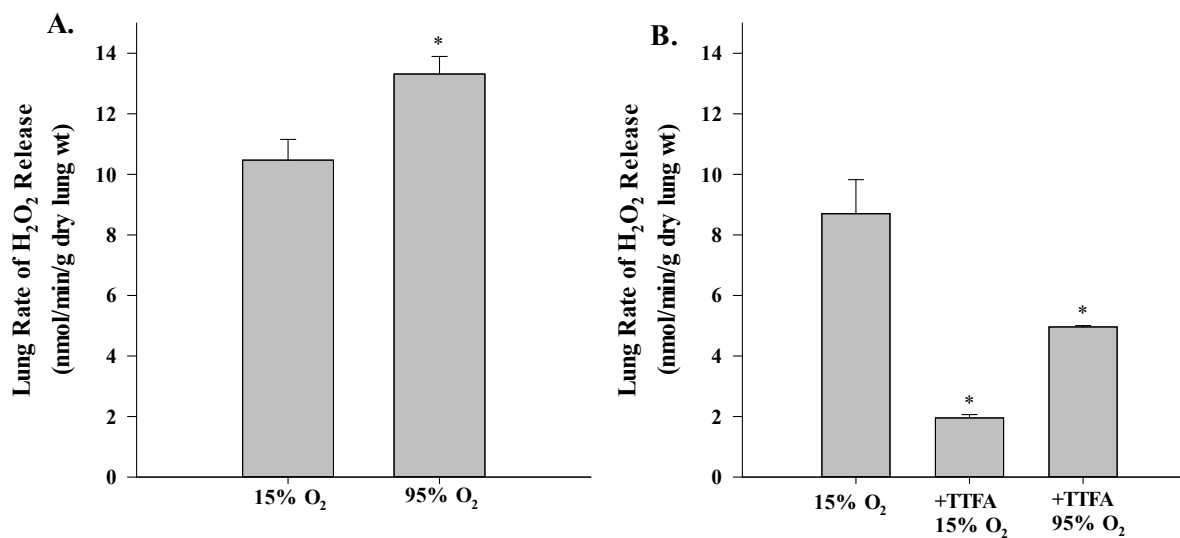


Figure 4.6: Effect of hyperoxia on H₂O₂ release Panel A: Rates of H₂O₂ release with isolated perfused lungs ($n = 4$) ventilated with a gas mixture of 15% O₂ or 95% O₂ (left). Panel B: Lung rate of H₂O₂ release in the presence of TTFA, with the lungs ventilated with 15% O₂ gas mixture or 95% O₂ gas mixture (right) ($N=4$). * paired t -test $p < 0.05$. Values are mean \pm SE.

CHAPTER 5: DISCUSSION AND CONCLUSIONS

5.1 Interpretation of Results

The present study describes a robust fluorometric approach for measuring the rate of H_2O_2 release from isolated perfused rat lungs, as an index of pulmonary oxidative stress, using the extracellular fluorescent probe Amplex Red (AR). For lungs from control rats, the results show that inhibiting mitochondrial complex II reduced this rate by ~76%, and inhibiting NOX reduced it by another ~23%. The results also show that inhibiting complex I had a small (13%), but significant effect on the rate, whereas inhibiting complex III had no significant effect on this rate. Furthermore, the results show that increasing % O_2 in the ventilation gas mixture from 15% to 95% O_2 had a relatively small (27%), but significant effect on this rate, and that this O_2 -dependent increase was mostly non-mitochondrial. As discussed below, these results suggest complex II as a potentially important source of ROS and a potential target for mitigating oxidative stress, and that most of the hyperoxia-enhanced lung rate H_2O_2 release is from NOX rather than mitochondrial sources. To the best of our knowledge, this is the first study measuring the rate of H_2O_2 release from isolated perfused rat lungs, identifying the main sources of this rate under physiological conditions, and evaluating the effect of acute hyperoxia on this rate.

The measured rate of H_2O_2 release is the net result of cellular ROS production and scavenging rates. However since the inhibitors used have no known effect on ROS scavenging rates under acute conditions, then changes in the measured rates of H_2O_2 release are reflective of changes in the rate of cellular ROS production.

According to Audi et al. the rat lung rate of oxygen consumption is ~ 2.4 $\mu\text{mol}/\text{min}/\text{g}$ dry lung wt. (Audi et al., 2003). The baseline lung rate of H_2O_2 release reported in this study under normoxic ventilation conditions (15% O_2 , 6% CO_2 , balance N_2) is 8.32 ± 0.32 (SE, $N = 33$) $\text{nmol}/\text{min}/\text{g}$ dry lung wt. Since superoxide to oxygen stoichiometry is 1:1 and superoxide to H_2O_2 stoichiometry is 2:1, then the oxygen equivalent rate of the measured lung rate of H_2O_2 release is 16.64 $\text{nmol}/\text{min}/\text{g}$ dry lung. This rate is $\sim 0.7\%$ of the rat lung rate of oxygen consumption and hence within the 1-2% of the total O_2 consumption rate that has been suggested to be converted to ROS production (Starkov, 2008).

Complex II oxidizes succinate to fumarate (Krebs cycle) and in the process reduces FAD to FADH_2 which in turn reduces ubiquinone to ubiquinol (electron transport chain, ETC) (Quinlan et al., 2012). Thus, complex II is unique in that it provides a direct link between the Krebs cycle and ETC, although it does not contribute directly to the generation of the proton motive force. As such, the main function of complex II is to help keep the quinone pool reduced. Unlike other complexes, all four subunits of complex II (the flavoprotein, the iron-sulfur protein, and the two transmembrane cytochrome b heme subunits) are encoded by nuclear DNA (Ide et al., 2001). An important and somewhat unexpected result is the large effect of inhibiting complex II on the lung rate of H_2O_2 release, and the relatively small effect of inhibiting complex I or complex III on this rate. TTFA inhibits complex II at the quinone reduction site (as seen in Figure 5.1). The effect of TTFA on the lung rate of H_2O_2 release could be due to complex II being an important source of ROS and/or via its effect on ROS production at complexes I and/or III (Dröse, 2013). One approach to assess the later possibility would be to evaluate the effect of

TFFA on the lung rate of H_2O_2 in the presence of complex I inhibitor (rotenone) and/or complex III inhibitor (antimycin A).

Studies using isolated mitochondria demonstrated that under certain experimental conditions (high succinate concentration and high mitochondrial membrane potential), complex II can enhance ROS production at complex I via reverse electron transfer from ubiquinol to complex I, and hence inhibition of complex II (or complex I) under such conditions leads to decrease in ROS production at complex I (Dröse, 2013). This is because inhibition of complex II (or complex I) reduces the membrane potential due to a decrease in the supply of reducing equivalents from complex II (or complex I) to complexes III and IV. On the other hand, under the same experimental conditions (high succinate and high mitochondrial membrane potential), inhibition of complex II can lead to an increase in ROS production at complex III in the presence of antimycin A which inhibits complex III at the Q_i subunit. Most studies with isolated mitochondria use high succinate concentrations (around 5 mM), which is a saturating concentration since the Michaelis-Menten (K_m) value for complex II and for the succinate transporter into mitochondria is around 1 mM (Quinlan et al., 2012). Normal tissue concentrations of succinate are in the sub-millimolar range. Quinlan et al. (2012) suggested that complex II may be a major source of ROS *in vivo*. They showed that complex II can be a major source of ROS under conditions of low succinate concentration (maximum rate at succinate concentration of $\sim 400 \mu\text{M}$, close to the physiological range) and inhibition of ubiquinone re-oxidation via complex I and III (i.e. in the presence of complex I and III inhibitors rotenone and myxothiazol, respectively). Both ubisemiquinone and FAD semiquinone radicals can be electron sources for the generation of ROS at complex II,

although evidence points to fully reduced FAD as the major source under such conditions. *These results suggest that the direct or indirect contribution of complex II to mitochondrial ROS production depends on substrate availability, mitochondrial membrane potential, and the activities of other ETC complexes.*

The large effect of the complex II inhibitor TTFA on the lung rate of H₂O₂ release suggests complex II as a potential target for mitigating oxidative stress. Under normal conditions, mitochondria account for ~80% of lung tissue ATP content. Bongard et al. showed that inhibiting complex I decreased the total lung ATP content by ~60%, whereas inhibiting complex I and III decreased total lung ATP content by ~70% (Bongard et al., 2013). This suggests that only ~10% of ATP lung content is complex II sensitive. The combination of its small effect on ATP content and large effect on lung rate of H₂O₂ release suggests complex II inhibition as a potential target for mitigating oxidative stress in lungs. This is consistent with a study by Valls-Lacalle et al. in which they showed that reversible inhibition of complex II with malonate at the start of reperfusion mitigated infarct size induced by ischemia-reperfusion injury in isolated mice hearts (Valls-Lacalle et al., 2016). They attributed this protection to reduction in a reperfusion-induced increase in mitochondrial ROS production, which contributes to mitochondrial permeability transition pore opening.

Results of the present study show that inhibiting complex I at the iron-sulfur groups with rotenone decreased the lung rate of H₂O₂ release by only 13%. The results also show that increasing % O₂ in the ventilation gas mixture from 15% to 95% O₂ had a relatively small (27%), but significant effect on the lung rate of H₂O₂ release, and this O₂-dependent increase was mostly non-mitochondrial, which is consistent with the fact that

NOX4 rate of ROS formation has a relatively large Michaelis-Menten constant ($K_m = \sim 18\%$) for O_2 (Nisimoto et al., 2014).

Results from previous studies regarding the effect of inhibiting complex I on mitochondrial ROS production have not been consistent, with some showing an increase, which others showing a decrease or no change in rate of ROS production (Brueckl et al., 2006; Ghanian, Konduri, Audi, Camara, & Ranji, 2018). Brueckl et al. measured the lung capillary endothelial cells ROS production in isolated perfused rat lungs using the intracellular fluorescent probe DCF with the lung ventilated with either normoxic gas mixture (21% O_2) or hyperoxic gas (up to 70% O_2) gas mixture. The lungs were perfused at 14 ml/min with heparinized autologous blood. The results show that DCF signal increased almost linearly with the % O_2 in the ventilation gas, which was varied between 21% and 70%. In addition, they showed that lung treatment with rotenone reduced baseline DCF signal (and hence baseline ROS production) by $\sim 60\%$ and completely inhibited hyperoxia-induced increase in DCF signal. These results, which suggest complex I as a major source of mitochondrial ROS, and almost linear relationship between mitochondrial ROS and % O_2 in ventilation gas, are not consistent with the results from the present study. This could be in part due to differences in the two probes used (DCF vs. Amplex Red). Due to the extracellular nature of AR, it cannot be used for measuring the actual lung rate of ROS production from a specific source since the measured rate is the net of cellular ROS production at multiple sources and ROS scavenging rates. Another potential reason for differences between the results of the study by Brueckl et al. and those of the present study is that in the present study the

measured rate of H₂O₂ is from the whole lung (all forty different types of cells) instead of from just capillary endothelial cells in the study by Brueckl et al.

Brueckl et al. (2006) also showed that DPI, an inhibitor of NOX, did not affect baseline DCF signal, but had a significant effect on hyperoxia-induced increase in DCF, especially towards the later phase of the 90-min exposure period. They suggested that the early phase of hyperoxia-induced increase in DCF signal was due to an increase in mitochondrial ROS, but the later phase of the hyperoxia-enhanced DCF signal was due to activation of NOX by endothelial calcium signaling and Rac1 activation. DPI's lack of effect on baseline DCF signal is not consistent with the effect of DPI on the lung rate of H₂O₂ release in the present study, although the contribution of NOX to hyperoxia-enhanced DCF signal is somewhat consistent the results from the present study.

Ghanian et al. measured the rate of superoxide production in cultured fetal lamb pulmonary artery endothelial cells using the fluorescence probe MitoSOX Red, a derivative of Hydroethidine (Ghanian et al., 2018). They showed that treatment of cells with rotenone increased superoxide production as measured by MitoSOX Red signal by ~60%. Additional results show that treatment of cells with antimycin A or potassium cyanide (KCN) also increased superoxide production by ~130% and 60%, respectively. The results with rotenone and antimycin A are inconsistent with the results of the present study or the study by Brueckl et al. (2006) with respect to the effect of rotenone on ROS production. Differences between cultured cells and organs and/or probes used could account for this apparent inconsistency. The increase in superoxide production in the presence of KCN reported by Ghanian et al. is consistent with the results in the present study, although the increase is smaller than the measured KCN-induced increase in the

lung rate of H₂O₂ release in the present study. Ghanian et al. concluded that complexes I, III and IV are major sources of superoxide in cultured pulmonary endothelial cells. The effect of KCN on the lung rate of H₂O₂ release in the present study could be indicative of complex IV being a source of ROS, especially since inhibiting complex III with antimycin A had no significant effect on this rate.

Using Amplex Red, Lee et al. (2013, 2014) measured the rate of H₂O₂ release by isolated perfused lungs from normal mice and from mice 24 hours after treatment with lipopolysaccharide (LPS) to induce lung injury (I. Lee et al., 2013; Intae Lee et al., 2014). They showed that LPS increased lung rate of H₂O₂ release by more than 9-fold and that ~90% of this increase was due to NOX 2. However, NOX 2 does not appear to contribute much to the baseline rate of lung H₂O₂ release. These results are somewhat consistent with results from the present study which show that ~75% of the lung rate of H₂O₂ release is from the mitochondria, and ~23% from NOX, potentially NOX 2 and/or NOX 4. For the above studies by Lee et al., the baseline rate of mouse lung H₂O₂ release was 0.0105 nmol/min/g dry lung, which is very small compared to the rate in rat lungs (8.3 nmol/min/g dry lung wt) in the present study. This could be due to species differences (Julie Turrens et al., 1982) and/or differences in the approach used to convert resorufin to H₂O₂. Lee et al. (2013 and 2014) used Amplex red's extinction coefficient (54,000 cm⁻¹ M⁻¹) to convert resorufin signal to H₂O₂ concentration, whereas in the present study a standard curve with known H₂O₂ concentrations was used to convert measured resorufin signal to H₂O₂ concentration in recirculating perfusate.

Antimycin A inhibits complex III at the Q_i subunit and this inhibits the transfer of electrons from heme b_H to oxidized Q (Huang et al., 2005). Thus, antimycin A locks the b

hemes in the reduced state by preventing their re-oxidation at the Q_i site, shown in Figure 5.1, causing the steady-state concentrations of the Q_o semiquinone to rise. Semiquinone reacts readily with oxygen to form superoxide and increase ROS production (Julio Turrens, Alexandria, & Lehninger, 1985). Previous studies have reported an increase in ROS production with the addition of antimycin A in reduced systems (e.g. cells and sub-mitochondrial particles) (Chen et al., 2003; Woo et al., 2007). Those results are not consistent with the results from the present study. Again, this could be to differences between reduced systems and intact functioning lung and/or differences between the probes used.

The complex IV inhibitor KCN increased the lung rate of H_2O_2 release by 310%. Increased ROS production in the presence of a complex IV inhibitor has been reported by other groups and has been shown to increase oxidative stress (Chen et al., 2003; Dawson, Gores, Nieminen, Herman, & Lemasters, 1993).

Cytosol

Outer Membrane

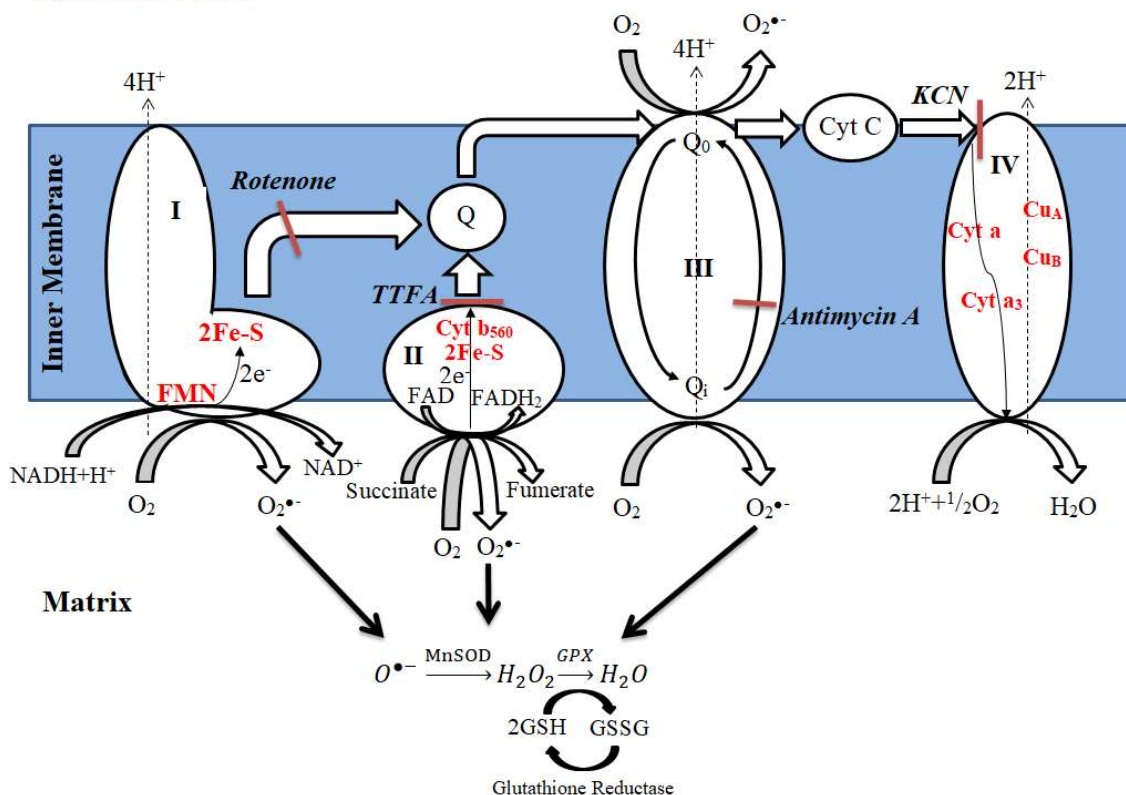


Figure 5.1: Schematic representation of mitochondrial ROS production and mitochondrial inhibitor sites.

In one lung, we assessed the rate of H₂O₂ release without the addition of HRP to the recirculating perfusate. The estimated rate of arbitrary fluorescence intensity increase (13,360 counts/s/min) was ~90% of that measured in the presence of HRP (14,855 counts/s/min) as shown in Figure 5.2. These preliminary results suggest that the capillary endothelial surface area has a relatively high peroxidase activity to catalyze the reaction of H₂O₂ with AR. This is consistent with the results of a study by Ryan et al. (Ryan &

Ryan, 1985) in which they demonstrated the presence of peroxidase activity on the capillary endothelial surface of rat lungs.

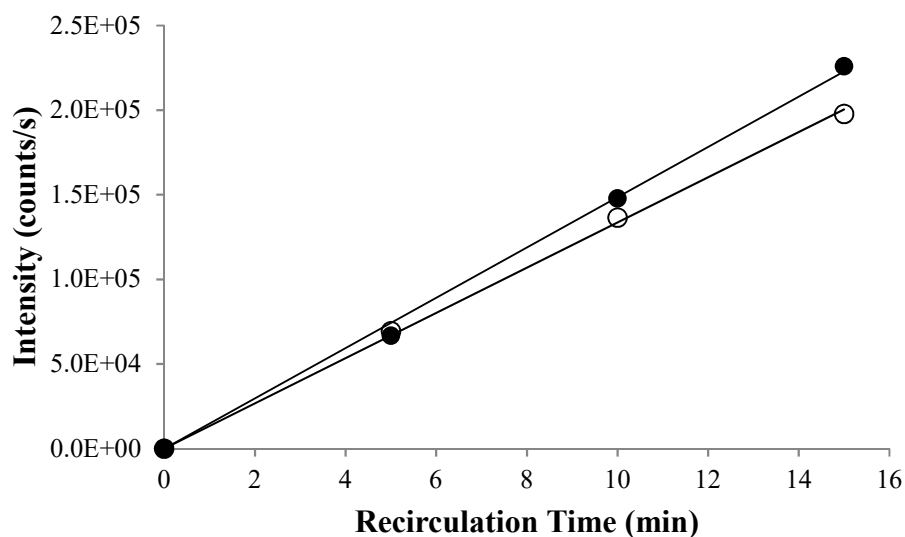


Figure 5.2: Arbitrary fluorescence measurement from recirculating lung samples with (●) and without (○) HRP.

5.2 Limitations of AR in the Isolated, Perfused Lung Preparation

Amplex Red (AR) provides a robust approach for measuring the rate of H_2O_2 release from isolated perfused lungs. However, this approach has several limitations. Due to the extracellular nature of AR, it cannot be used to measure the actual lung rate of ROS production or the rate of production from a specific source since the measured rate is the net of the rates of cellular ROS production and ROS scavenging, and since a given inhibitor can affect ROS production at multiple sources as discussed above. Quinlan et al.

(2012) proposed an empirical approach for correcting for the effect of ROS scavenging on the measured rate of H₂O₂ release.

The lung consists of 40 different cell types. The results using AR provide no direct information regarding the contributions of the different cell types to the measured lung rate of H₂O₂ release, although endothelial cells would be expected to dominate because of their large surface area and high fraction (~50%) of total lung cells, and their direct contact with AR in perfusate. Although the question regarding the contributions of specific cell types will be important for future studies, alteration in the lung rate of H₂O₂ release as an index of pulmonary oxidative stress has functional implications regardless of the lung cell types involved.

Another potential limitation for the use of AR in isolated perfused lungs is that the contribution of a given cellular source to the measured rate of H₂O₂ release may depend not only on its rate of ROS production, but also on its location within the cell. Superoxide and H₂O₂ from ETC are in close proximity to many antioxidants, whereas those from NOX are in direct contact with perfusate and hence may contribute proportionately more to the measured lung rate of H₂O₂ release.

It is also important to note that the interactions of the inhibitor vehicles with the fluorescence signal were evaluated to ensure that measured change in signal is due to the inhibitor itself rather than the vehicle (Figure 4.1). Neither the potassium phosphate buffer nor DMSO showed significant change on resorufin signal at the volumes used. However, DMSO does have antioxidant capabilities at high concentrations, and thus it is important to keep the volume of DMSO added to the recirculation perfusate at < 0.1% of

the perfusate volume (0.05% in the present study) (Sanmartín-Suárez, Soto-Otero, Sánchez-Sellero, & Méndez-Álvarez, 2011).

The conclusion regarding the contribution of a given cellular source to the measured lung rate of H₂O₂ release could be strengthened by demonstrating similar changes in the measured rate using different pharmacological inhibitors of this cellular source and/or using genetically manipulations to downregulate the activity of this cellular source.

5.3 Conclusions

To the best of our knowledge, this study is the first to evaluate the rate of H₂O₂ production in the isolated perfused rat lung and to determine the contributions of mitochondrial and non-mitochondrial sources of ROS to the measured rate. This approach could be used to assess the role of oxidative stress in the pathogenesis of ALI/ARDS and the efficacy of novel therapies for mitigating oxidative stress in intact functioning lungs.

BIBLIOGRAPHY

- Andreyev, a Y., Kushnareva, Y. E., & Starkov, a a. (2005). Mitochondrial metabolism of reactive oxygen species. *Biochemistry. Biokhimiia*, 70(2), 200–214. <https://doi.org/BCM70020246> [pii]
- Audi, S. H., Bongard, R. D., Dawson, C. a, Siegel, D., Roerig, D. L., & Merker, M. P. (2003). Duroquinone reduction during passage through the pulmonary circulation. *American Journal of Physiology. Lung Cellular and Molecular Physiology*, 285(5), L1116-31. <https://doi.org/10.1152/ajplung.00185.2003>
- Audi, S. H., Bongard, R. D., Okamoto, Y., Merker, M. P., Roerig, D. L., & Dawson, C. A. (2001). Pulmonary reduction of an intravascular redox polymer. *Am J Physiol Lung Cell Mol Physiol*, 280(6), L1290-9. Retrieved from http://www.ncbi.nlm.nih.gov/entrez/query.fcgi?cmd=Retrieve&db=PubMed&dopt=Citation&list_uids=11350810
- Audi, S., Jacobs, E., Zhao, M., Roerig, D., Haworth, S., & Clough, A. (2001). In vivo detection of hyperoxia-induced pulmonary endothelial cell death using 99mTc-Duramycin. *AJP: Lung Cellular and Molecular Physiology*, 280, L1290–L1299.
- Audi, S., Jacobs, E., Zhao, M., Roerig, D., Haworth, S., & Clough, A. (2015). In Vivo Detection of Hyperoxia-Induced Pulmonary Endothelial Cell Death Using 99mTc-Duramycin. *Nucl Med Biol.*, 42(1), 46–52. <https://doi.org/10.1002/nbm.3369>.Three
- Barrientos, A., & Moraes, C. T. (1999). Titrating the effects of mitochondrial complex I impairment in the cell physiology. *Journal of Biological Chemistry*, 274(23), 16188–16197. <https://doi.org/10.1074/jbc.274.23.16188>
- Bayir, H., & Kagan, V. (2008). Bench-to-bedside review: Mitochondrial injury, oxidative stress and apoptosis, there is nothing more practical than a good theory. *Critical Care*, 12(1), 206.
- Bienert, G. P., Schjoerring, J. K., & Jahn, T. P. (2006). Membrane transport of hydrogen peroxide. *Biochimica et Biophysica Acta (BBA) - Biomembranes*, 1758(8), 994–1003. <https://doi.org/10.1016/j.bbamem.2006.02.015>
- Bongard, R., Yan, K., Hoffmann, R., Audi, S., Zhang, X., Lindemer, B., ... Merker, M. (2013). Depleted energy charge and increased pulmonary endothelial permeability induced by mitochondrial complex I inhibition are mitigated by coenzyme Q1 in the isolated perfused rat lung. *Free Radic Biol Med.*, 65, 1455–1463. <https://doi.org/10.1016/j.freeradbiomed.2013.07.040>.Depleted
- Brueckl, C., Kaestle, S., Kerem, A., Habazettl, H., Krombach, F., Kuppe, H., & Kuebler, W. M. (2006). Hyperoxia-induced reactive oxygen species formation in pulmonary capillary endothelial cells in situ. *American Journal of Respiratory Cell and Molecular Biology*, 34(4), 453–463. <https://doi.org/10.1165/rcmb.2005-0223OC>

- Campian, J. L., Qian, M., Gao, X., & Eaton, J. W. (2004). Oxygen tolerance and coupling of mitochondrial electron transport. *The Journal of Biological Chemistry*, 279(45), 46580–7. <https://doi.org/10.1074/jbc.M406685200>
- Chatterjee, S., Chapman, K. E., & Fisher, A. B. (2008). Lung ischemia: A model for endothelial mechanotransduction. *Cell Biochemistry and Biophysics*, 52(3), 125–138. <https://doi.org/10.1007/s12013-008-9030-7>
- Chatterjee, S., Feinstein, S., Dodia, C., Sorokina, E., Lien, Y.-C., Nguyen, S., ... Fisher, A. (2011). Peroxiredoxin 6 Phosphorylation and Subsequent Phospholipase A2 Activity Are Chatterjee, S., Feinstein, S., Dodia, C., Sorokina, E., Lien, Y.-C., Nguyen, S., ... Fisher, A. (2011). Peroxiredoxin 6 Phosphorylation and Subsequent Phospholipase A2 Activity Are. *Journal of Biological Chemistry*, 286(13), 11696–11706.
- Chen, Q., Vazquez, E. J., Moghaddas, S., Hoppel, C. L., & Lesnefsky, E. J. (2003). Production of reactive oxygen species by mitochondria: Central role of complex III. *Journal of Biological Chemistry*, 278(38), 36027–36031. <https://doi.org/10.1074/jbc.M304854200>
- Chiang, C.-H., Chuang, C.-H., Liu, S.-L., Lee, T.-S., & Zhang, H. (2011). Apocynin attenuates lipopolysaccharide-induced lung injury in an isolated and perfused rat lung model. *Shock (Augusta, Ga.)*, 38(2), 196–202. <https://doi.org/10.1097/SHK.0b013e31825a1982>
- Cifuentes-Pagano, E., Meijles, D. N., & Pagano, P. J. (2014). The Quest for Selective Nox Inhibitors and Therapeutics: Challenges, Triumphs and Pitfalls. *Antioxidants & Redox Signaling*, 20(17), 2741–2754. <https://doi.org/10.1089/ars.2013.5620>
- Dawson, T. L., Gores, G. J., Nieminen, a L., Herman, B., & Lemasters, J. J. (1993). Mitochondria as a source of reactive oxygen species during reductive stress in rat hepatocytes. *The American Journal of Physiology*, 264(4 Pt 1), C961-7. Retrieved from <http://www.ncbi.nlm.nih.gov/pubmed/8386454>
- Dikalov, S. I., & Harrison, D. G. (2014). Methods for Detection of Mitochondrial and Cellular Reactive Oxygen Species. *Antioxidants & Redox Signaling*, 20(2), 372–382. <https://doi.org/10.1089/ars.2012.4886>
- Dröse, S. (2013). Differential effects of complex II on mitochondrial ROS production and their relation to cardioprotective pre- and postconditioning. *Biochimica et Biophysica Acta - Bioenergetics*, 1827(5), 578–587. <https://doi.org/10.1016/j.bbabi.2013.01.004>
- Freeman, B., Topolosky, M., & Crapo, J. (1982). Hyperoxia increases oxygen radical production in rat lung homogenates. *Archives of Biochemistry and Biophysics*, 216(2), 477–484.
- Ghanian, Z., Konduri, G. G., Audi, S. H., Camara, A. K. S., & Ranji, M. (2018). Quantitative optical measurement of mitochondrial superoxide dynamics in

- pulmonary artery endothelial cells. *Journal of Innovative Optical Health Sciences*, 11(1), 1–16. <https://doi.org/10.1142/S1793545817500183>
- Goncalves, R. L. S., Quinlan, C. L., Perevoshchikova, I. V., Hey-Mogensen, M., & Brand, M. D. (2015). Sites of superoxide and hydrogen peroxide production by muscle mitochondria assessed ex vivo under conditions mimicking rest and exercise. *Journal of Biological Chemistry*, 290(1), 209–227. <https://doi.org/10.1074/jbc.M114.619072>
- Griffith, B., Pendyala, S., Hecker, L., Lee, P., Natarajan, V., & Thannickal, V. (2009). NOX Enzymes and Pulmonary Disease. *Antioxidants & Redox Signaling*, 11(10), 2502–2516. <https://doi.org/10.1089/ars.2010.3397>
- Haffner, S. (2000). Oxidative stress: Introduction. *Metabolism*, 58(1), 1–2.
- Hirano, K., Chen, W. S., Chueng, A. L. W., Dunne, A. A., Seredenina, T., Filippova, A., ... Rutter, A. R. (2015). Discovery of GSK2795039, a Novel Small Molecule NADPH Oxidase 2 Inhibitor. *Antioxidants & Redox Signaling*, 23(5), 358–374. <https://doi.org/10.1089/ars.2014.6202>
- Hoekstra, A. S., & Bayley, J. P. (2013). The role of complex II in disease. *Biochimica et Biophysica Acta - Bioenergetics*, 1827(5), 543–551. <https://doi.org/10.1016/j.bbabi.2012.11.005>
- Huang, L., Cobessia, D., Tung, E., & Berry, E. (2005). Binding of the respiratory chain inhibitor antimycin to the mitochondrial bc1 complex: a new crystal structure reveals an altered intramolecular hydrogen-binding pattern. *J Mol Biol*, 351(3), 573–597. <https://doi.org/10.1016/j.immuni.2010.12.017>. Two-stage
- Ide, T., Tsutsui, H., Hayashidani, S., Kang, D., Suematsu, N., Nakamura, K., ... Takeshita, a. (2001). Mitochondrial DNA damage and dysfunction associated with oxidative stress in failing hearts after myocardial infarction. *Circulation Research*, 88, 529–535. <https://doi.org/10.1161/01.RES.88.5.529>
- Instruments, B., & Park, H. (2006). Quantitation of Hydrogen Peroxide using the Synergy HT™, 2–7.
- Kallet, R., & Matthay, M. (2012). Hyperoxic Acute Lung Injury. *Respiratory Care*, 58(1), 123–141.
- Kalyanaramana, Balaraman Darley-Usmarb, V., J.A. Davies, K., Dennerly, P. A., Forman, H. J., Grisham, M. B., Mann, G. E., ... Ischiropoulos, H. (2013). Measuring reactive oxygen and nitrogen species with fluorescent probes: challenges and limitations. *Free Radical Biology and Medicine*, 45(4), 1–6. <https://doi.org/10.1016/j.freeradbiomed.2011.09.030>. Measuring
- Kinnula, V., Chang, L., Ho, Y., & Crapo, J. (1992). Hydrogen peroxide release from alveolar macrophages and alveolar type II cells during adaptation to hyperoxia in vivo. *Experimental Lung Research*, 18(5), 655–673.

- Klebanoff, S. (2005). Myeloperoxidase: friend and foe. *Journal of Leukocyte Biology*, 77(5), 598–625.
- Koziel, A., Sobieraj, I., & Jarmuszkiewicz, W. (2015). Increased activity of mitochondrial uncoupling protein 2 improves stress resistance in cultured endothelial cells exposed in vitro to high glucose levels. *American Journal of Physiology - Heart and Circulatory Physiology*, 309(1), H147–H156. <https://doi.org/10.1152/ajpheart.00759.2014>
- Kühlbrandt, W. (2015). Structure and function of mitochondrial membrane protein complexes. *BMC Biology*, 13(1), 89. <https://doi.org/10.1186/s12915-015-0201-x>
- Kumar, G., Kumar, N., Taneja, A., Kaleekal, T., Tarima, S., McGinley, E., ... Nanchal, R. (2011). Nationwide trends of severe sepsis in the 21st century (2000-2007). *Chest*, 140(5), 1223–1231. <https://doi.org/10.1378/chest.11-0352>
- Lee, I., Dodia, C., Chatterjee, S., Feinstein, S., & Fisher, A. (2014). Protection against LPS-induced acute lung injury by a mechanism-based inhibitor of NADPH oxidase (type 2). *AJP: Lung Cellular and Molecular Physiology*, 306(7), L635–L644.
- Lee, I., Dodia, C., Chatterjee, S., Zagorski, J., Mesaros, C., Blair, I. A., ... Fisher, A. B. (2013). A Novel Nontoxic Inhibitor of the Activation of NADPH Oxidase Reduces Reactive Oxygen Species Production in Mouse Lung. *Journal of Pharmacology and Experimental Therapeutics*, 345(2), 284–296. <https://doi.org/10.1124/jpet.112.201079>
- Li, N., Ragheb, K., Lawler, G., Sturgis, J., Rajwa, B., Melendez, J. A., & Robinson, J. P. (2003). Mitochondrial complex I inhibitor rotenone induces apoptosis through enhancing mitochondrial reactive oxygen species production. *Journal of Biological Chemistry*, 278(10), 8516–8525. <https://doi.org/10.1074/jbc.M210432200>
- Matthay, M., Ware, L., & Zimmerman, G. (2012). The acute respiratory distress syndrome. *Journal of Clinical Investigation*, 122(8), 2731–2740.
- Mittal, M., Siddiqui, M. R., Tran, K., Reddy, S. P., & Malik, A. B. (2014). Reactive Oxygen Species in Inflammation and Tissue Injury. *Antioxidants & Redox Signaling*, 20(7), 1126–1167. <https://doi.org/10.1089/ars.2012.5149>
- Muller, F. (2000). The nature and mechanism of superoxide production by the electron transport chain: Its relevance to aging. *Journal of the American Aging Association*, 23(4), 227–53. <https://doi.org/10.1007/s11357-000-0022-9>
- Murphy, M. P. (2008a). How mitochondria produce reactive oxygen species. *Biochemical Journal*, 417(1), 1 LP-13. Retrieved from <http://www.biochemj.org/content/417/1/1.abstract>
- Murphy, M. P. (2008b). How mitochondria produce reactive oxygen species. *Biochemical Journal*, 417(1), 1 LP-13.
- Nisimoto, Y., Diebold, B. A., Constantino-Gomes, D., & Lambeth, J. D. (2014). Nox4: A

- hydrogen peroxide-generating oxygen sensor. *Biochemistry*, 53(31), 5111–5120. <https://doi.org/10.1021/bi500331y>
- Paddenberg, R., Ishaq, B., Goldenberg, A., Faulhammer, P., Rose, F., Weissmann, N., ... Kummer, W. (2003). Essential role of complex II of the respiratory chain in hypoxia-induced ROS generation in the pulmonary vasculature. *American Journal of Physiology. Lung Cellular and Molecular Physiology*, 284(5), L710-9. <https://doi.org/10.1152/ajplung.00149.2002>
- Quinlan, C. L., Orr, A. L., Perevoshchikova, I. V., Treberg, J. R., Ackrell, B. A., & Brand, M. D. (2012). Mitochondrial complex II can generate reactive oxygen species at high rates in both the forward and reverse reactions. *Journal of Biological Chemistry*, 287(32), 27255–27264. <https://doi.org/10.1074/jbc.M112.374629>
- Rhee, S. G., Chang, T.-S., Jeong, W., & Kang, D. (2010). Methods for detection and measurement of hydrogen peroxide inside and outside of cells. *Molecules and Cells*, 29(6), 539–549.
- Rodrigues, J., & Gomes, C. (2010). Enhanced superoxide and hydrogen peroxide detection in biological assays. *Free Radical Biology and Medicine*, 49(1), 61–66.
- Ryan, U., & Ryan, J. (1985). The site and mechanism of oxygen sensing for the pulmonary vessels. *Chest*, 88(4), 203S–207S. <https://doi.org/10.1378/chest.88.4>
- Sanders, S. P., Zweier, J. L., Kuppusamy, P., Harrison, S. J., Bassett, D. J., Gabrielson, E. W., & Sylvester, J. T. (1993). Hyperoxic sheep pulmonary microvascular endothelial cells generate free radicals via mitochondrial electron transport. *The Journal of Clinical Investigation*, 91(1), 46–52. <https://doi.org/10.1172/JCI116198>
- Sanmartín-Suárez, C., Soto-Otero, R., Sánchez-Sellero, I., & Méndez-Álvarez, E. (2011). Antioxidant properties of dimethyl sulfoxide and its viability as a solvent in the evaluation of neuroprotective antioxidants. *Journal of Pharmacological and Toxicological Methods*, 63(2), 209–215. <https://doi.org/10.1016/j.vascn.2010.10.004>
- Sepehr, R., Audi, S. H., Staniszewski, K. S., Haworth, S. T., Jacobs, E. R., & Ranji, M. (2013). Novel Fluorometric Tool to Assess Mitochondrial Redox State of Isolated Perfused Rat Lungs After Exposure to Hyperoxia, 1(May).
- Song, C., Al-Mehdi, A., & Fisher, A. B. (2001). An immediate endothelial cell signaling response to lung ischemia. *American Journal of Physiology. Lung Cellular and Molecular Physiology*, 281(4), L993–L1000.
- Starkov, A. A. (2008). The role of mitochondria in reactive oxygen species metabolism and signalling. *Ann. NY Acad. Sci.*, 1147, 37–52. <https://doi.org/10.1196/annals.1427.015>
- Turrens, J. (2003). Mitochondrial formation of reactive oxygen species. *The Journal of Physiology*, 552(2), 335–344. <https://doi.org/10.1113/jphysiol.2003.049478>
- Turrens, J., Alexandria, A., & Lehninger, A. (1985). Ubisemiquinone is the electron

- donor for superoxide formation by complex III of heart mitochondria. *Archives of Biochemistry and Biophysics*, 237(1), 408–414.
- Turrens, J., Freeman, B., & Crapo, J. (1982). Hyperoxia increases H₂O₂ release by lung mitochondria and microsomes. *Archives of Biochemistry and Biophysics*, 217(2), 411–421.
- Valls-Lacalle, L., Barba, I., Miró-Casas, E., Albuquerque-Béjar, J. J., Ruiz-Meana, M., Fuertes-Agudo, M., ... García-Dorado, D. (2016). Succinate dehydrogenase inhibition with malonate during reperfusion reduces infarct size by preventing mitochondrial permeability transition. *Cardiovascular Research*, 109(3), 374–384. <https://doi.org/10.1093/cvr/cvv279>
- Weissmann, N., Kuzkaya, N., Fuchs, B., Tiyerili, V., Schäfer, R. U., Schütte, H., ... Grimminger, F. (2005). Detection of reactive oxygen species in isolated, perfused lungs by electron spin resonance spectroscopy. *Respiratory Research*, 6(1), 86. <https://doi.org/10.1186/1465-9921-6-86>
- Woo, H. P., Yong, W. H., Suh, H. K., & Sung, Z. K. (2007). An ROS generator, antimycin A, inhibits the growth of HeLa cells via apoptosis. *Journal of Cellular Biochemistry*, 102(1), 98–109. <https://doi.org/10.1002/jcb.21280>
- Zhang, D. X., & Gutterman, D. D. (2007a). Mitochondrial reactive oxygen species-mediated signaling in endothelial cells. *American Journal of Physiology - Heart and Circulatory Physiology*, 292(5). Retrieved from <http://ajpheart.physiology.org/content/292/5/H2023>
- Zhang, D. X., & Gutterman, D. D. (2007b). Mitochondrial reactive oxygen species-mediated signaling in endothelial cells. *American Journal of Physiology - Heart and Circulatory Physiology*, 292(5).
- Zhao, B., Summers, F., & Mason, R. (2012). Photooxidation of Amplex red to resorufin: Implications of exposing the Amplex red assay to light. *Free Radical Biology and Medicine*, 53(5), 1080–1087.
- Zhou, M., Diwu, Z., Panchuk-Voloshina, N., & Haugland, R. (1997). A Stable Nonfluorescent Derivative of Resorufin for the Fluorometric Determination of Trace Hydrogen Peroxide: Applications in Detecting the Activity of Phagocyte NADPH Oxidase and Other Oxidases. *Analytical Biochemistry*, 253(2), 162–168.

APPENDIX

A. Preparation of Stock solutions:

- *Amplex Red (AR):*

The 5 mg powder purchased from Sigma Aldrich (catalog # 90101) is first brought to room temperature. DMSO is used as the solvent for AR. A concentration of 20 mM AR stock is achieved by adding 0.97 ml of DMSO to the 5 mg of AR. First, 0.5 ml DMSO is added to the AR tube, the solution is mixed well using a vortex genie, and the 0.5 ml is transferred to 1.6 mL centrifuge tube. Next, 0.47 mL of DMSO is added to the AR tube, the solution is mixed well, and transferred to the enppendorf tube that contains the rest of the AR solution.

Once the 20 mM AR stock is prepared, fractionation into small samples is required. 70 μ L of AR stock is added to each 0.2 mL centrifuge tube. The samples are then frozen at -20°C for later use.

- *Horseradish peroxidase (HRP):*

Hydrolyzed powder of HRP (Sigma Aldrich, St. Louis, MO, P8375) refrigerated at 4°C. Before each experiment, the powder is brought to room temperature before preparing the stock solution.

Stock solution of HRP is prepared by measuring 2 mg of HRP, which is dissolved in 1 mL of deionized water in a 1.6 mL centrifuge tube (500 U/ml). The solution is then mixed well using a vortex genie.

- *Ascorbate oxidase (AO):*

Ascorbate oxidase (Sigma Aldrich, St. Louis, MO, A0157) must be dissolved in a phosphate buffer solution for fractionation. The fractionation procedure is listed below.

- 1) Obtain all necessary materials:

- a. Ascorbate oxidase
- b. Na_2HPO_4
- c. NaH_2PO_4
- d. BSA
- e. Deionized water
- f. Two 50mL beakers
- g. Two small magnetic stir bars
- h. Two stir plates
- i. Two 10 mL tube with caps
- j. 1.6 mL centrifuge tube
- k. Ten 0.65mL centrifuge tubes

- 2) Prepare 20 mL of 1 M Na_2HPO_4 .

- a. Measure 2.84 g of Na_2HPO_4 .
- b. Place into a 50 mL beaker labelled ' Na_2HPO_4 '.
- c. Add 20 mL of deionized water.
- d. Add a small stir bar.
- e. Place the solution on a stir plate and stir until completely dissolved.

- 3) Prepare 20 mL of 1 M NaH_2PO_4
 - a. Measure 2.76 g of NaH_2PO_4 .
 - b. Place into a 50 mL beaker labelled ' NaH_2PO_4 '.
 - c. Add 20 mL of deionized water.
 - d. Add a small stir bar.
 - e. Place the solution on a stir plate and stir until completely dissolved.
- 4) Prepare a 1M phosphate buffer with a pH of 5.6.
 - a. Transfer 9.21mL of the 1M NaH_2PO_4 to a 10mL tube labelled 1M.
 - b. Transfer 0.79 mL of the 1M Na_2HPO_4 to the same 10mL tube labelled 1 M.
- 5) Make a 4 mM buffer with 0.05% BSA
 - a. Add 10 mL of deionized water to a 10mL tube labelled 4 mM.
 - b. Add 40 μL of the 1M phosphate buffer to the same 10 mL tube labelled 4 mM.
 - c. Weigh 5 mg of BSA and add it to the same 10 mL tube labelled 4 mM.
 - d. Cap and mix the solution until the BSA is fully dissolved.
- 6) Transfer 0.5 mL of the 4 mM buffer into the AO container
- 7) Cap the AO container and mix well.
- 8) Transfer all liquid into a 1.6 mL centrifuge tube.
- 9) Repeat steps 6-8 (final volume of 1 mL).

- 10) Cap and mix the AO solution well.
- 11) Add 100 μ L of the AO solution to each of the ten 0.65mL Centrifuge tubes.
- 12) Freeze the samples for later use in experiments.

- Preparation of inhibitor stock solutions:

Each inhibitor is made prior to the experiment with the specified concentrations and solvents listed below. All inhibitors have been tested for interactions with Amplex Red and resorufin.

Table A.1: List of inhibitors used in experimental protocols with the corresponding stock concentration, solvent, volume of the stock added to 25 mL of perfusate, and the final concentration of the inhibitor in 25 mL perfusate.

Inhibitor	Stock Conc.	Solvent	Stock volume for 25mL perfusate	Inhibitor conc. in 25mL
Rotenone	100 mM	DMSO	10 μ l	40 μ M
TTFA	40 mM	DMSO	12.5 μ l	20 μ M
Antimycin A	18.8 mM	95% Ethanol	5 μ l	3.76 μ M
KCN	1 M	0.2 M KH ₂ PO ₄	50 μ l	2mM
DPI	15.8 mM	DMSO	7.9 μ l	5 μ M

- *Hydrogen peroxide for standard curve solutions (0.2 mM):*

Remove stock 30% H₂O₂ (Sigma Aldrich, St. Louis, MO, 216763) from the refrigerator and allow it to warm to room temperature. Prepare two 12 mL test tubes with one labelled 49 mM H₂O₂ and the other labelled 0.2 mM H₂O₂. Add 10 mL of deionized water to both test tubes.

Pipette 50 μL of 30% H_2O_2 into the tube labeled 49 mM H_2O_2 . Cap the tube and mix thoroughly using the vortex genie. Pipette 41 μL of 49 mM H_2O_2 into the 0.2 mM H_2O_2 tube. Cap the tube and mix thoroughly using the vortex genie. The 0.2 mM H_2O_2 tube is then used for the standard curve measurement.

B. PTI Software Setup

- 1) Open the Felix software.
- 2) Select the Amplex red macro.
- 3) Select 'Set up'.
- 4) Select 'Time based'
- 5) Select the acquisition settings tab in the set up window.
- 6) Switch the excitation wavelength to 545nm.
- 7) Change the acquisition time to 250 seconds.

C. Experimental setup:

All of the materials that must be gathered for an experiment are listed below. For specific experiments (e.g. perfusion with rotenone), extra preparation and materials may be needed.

- 1) Solutions:
 - a. Horseradish peroxidase (2mg/mL prepared, 250 μL per 25mL perfusate)
 - b. Amplex Red (70 μl tubes, 0.5 tube per lung and 0.5 tube per standard curve)
 - c. Ascorbate Oxidase (100 μL per 25 mL perfusate)
 - d. 3% BSA perfusate (~100 mL per lung)
 - e. 0.2 mM hydrogen peroxide

D. Background measurement procedure:

Background experiments were performed several times to establish an average rate of increase due to auto-oxidation in the perfusion system. Measurement is completed with the same perfusate, but without a lung attached to the ventilation-perfusion system.

The procedure is detailed below:

- 1) Gather all materials and complete steps specified in the experimental setup.
- 2) Setup software with the procedure described earlier.
- 3) Ensure AR, HRP, and AO are prepared in correct volumes and placed in a drawer with known positions to make each easy to find in the dark.
- 4) Set pipettes to the correct volume and cap each with clean tips.
 - a. 100 μ L pipette to 100 μ L for the AO
 - b. 1mL pipette to 0.25 mL for the HRP
 - c. 100 μ L pipette to 31.25 μ L for the AR
- 5) Measure 20mL of perfusate using a 25mL graduated cylinder
- 6) Transfer the perfusate to a 50mL tube and bring into the experiment room.
- 7) Turn off room lights and turn on a red lamp.
- 8) Turn on the ASOC.
- 9) Test the system for blank measurement:
 - a. Click 'Play' on the Felix software.
 - b. Look for a green light in the cuvette and a >100,000 counts/sec measurement.

- c. Add an event to note the end of the test period and beginning of the first sample.
- 10) If the software test passes, begin the experiment. Otherwise, software troubleshooting is required before the experiment can begin.
- 11) Make the perfusate:
 - a. Add 100 μL of AO stock
 - b. Add 0.25 mL of HRP stock
 - c. Add 31.25 μL of AR stock
- 12) Cap and invert the tube several times to mix the perfusate.
- 13) Stop the flow of the recirculating perfusate and use the large syringe to remove all liquid from the reservoir.
- 14) Pour the prepared perfusate into the reservoir
- 15) Set up a stop watch for timing.
- 16) Begin circulation and stopwatch timing at the same time.
- 17) Wait 45 seconds and restart the stopwatch.
- 18) Take two 1mL samples in two 1.6mL centrifuge tubes.
- 19) Place the two 1mL samples opposite of each other in the centrifuge.
- 20) Start the centrifuge for 1 minute at 13,000 g's and 4°C.
- 21) Remove the samples from the centrifuge.
- 22) Pipette the samples from the tubes and into the clean cuvette
- 23) Cap the cuvette.
- 24) Press 'Play' on the Felix software to begin sampling.

- 25) Sample for 10 seconds and then press 'Pause' on the Felix software to end sampling.
- 26) Add an event to note the end of the sampling period and record the time intervals in the lab notebook.
- 27) Record the approximate intensity in counts/sec in the lab notebook.
- 28) Transfer the sample back into the reservoir,
- 29) Add 2 mL of deionized water to the cuvette to wash
- 30) Discard all liquid in the cuvette into the waste beaker.
- 31) Repeat steps 18-30 for each time point (5, 10, 20, and 30 minutes).
- 32) Once all samples are recorded, press 'Stop' on the Felix software.
- 33) Turn the ASOC off.
- 34) Turn on the room light and the red lamp off.
- 35) Export the trace to a text file for later analysis.

E. Standard curve procedure:

Label four 5 mL tubes (with caps) 0, 1, 2, and 3. Pipette 4 mL of prepared BSA perfusate into each tube. Pipette 40 μL of prepared HRP into each tube. Cap each tube and mix briefly with a vortex genie. Move samples into the imaging room with the experimental and software setup completed along with 20 μL of stock AR, and the prepared 0.2 mM H_2O_2 tube.

To prepare each sample, 5 μL of AR are added along with the appropriate amount of 0.2 mM H_2O_2 for each concentration (20 μl for 1 μM , 40 μl for 2 μM , and 60 μl for 3 μM). If another chemical's interaction with AR/resorufin is tested, the chemical is also added in the appropriate concentration. After everything is added to the tube, the tube is

capped and inverted several times to ensure AR has fully reacted with the H_2O_2 present. Two 1 mL samples are pipetted from the tube and into two 1.6 mL centrifuge tubes. The samples are then centrifuged at 13,000 g's for 1 minute at 4°C.

After centrifugation, the 1 mL samples are pipetted from the centrifuge tube and into the clean cuvette. 'Play' is pressed on the Felix software to begin sampling. Sampling continues for 10 seconds and then 'Pause' is pressed on the Felix software to end sampling. The liquid in the cuvette is discarded, 2 mL of deionized water is added to the cuvette to wash, and the water is discarded.

Once all samples are recorded, 'Stop' is pressed on the Felix software, the ASOC is turned off, and the lights may be turned on. The trace is then exported to a text file for later analysis.

For a given inhibitor, the above standard curve will be repeated with the inhibitor added to the samples prior to the addition of H_2O_2 to make sure that neither inhibitor, nor the vehicle, interferes with the resorufin signal.

Data Analysis:

- 1) Import each exported text file into its own sheet on an Excel file created for the day's experiments
 - i) One sheet per lung tested.
 - ii) One sheet for the standard.
 - iii) One sheet for the background run if completed.
- 2) Complete the analysis for the standard measurement to obtain the rate of intensity increase per μM of H_2O_2 .

i) Use events marked during the experiments to identify the range of samples of each concentration. Highlight the rows for the times marked as events.

ii) Create a row of column labels as shown below:

[H2O2]	Fluor	[O] Removed
0	379683.1	0.00
1	1309027	929344.3319
2	2010843	1631159.638
3	2762027	2382343.494

iii) If another condition was tested (e.g. with rotenone), create another table for the condition.

iv) The 4 rows under column '[H2O2]' should always read 0, 1, 2, and 3.

v) In the 'Fluor' column, take the average of the samples recorded for respective H₂O₂ concentration sample time range.

vi) Subtract the fluorescence measured at a concentration of 0 from the raw fluorescence measurement in column 2 for the value for column 3 ('[O] Removed')

vii) Plot column 3 vs. column 1 as a scatter plot

viii) Add trend line

(1) Select set intercept to (0,0)

(2) Select display equation on chart

ix) Use the slope as the rate of fluorescence increase per μM increase in H₂O₂

3) Background measurement data processing

i) Write a row with the following column headings:

Time	Fluor	t0 removed	microM	nmol
0	212134.2	0	0	0
10	288956.1	76821.91216	0.148623	3.715583
20	370736.5	158602.2398	0.306839	7.670986
25	406444.6	194310.4153	0.375922	9.398054

- ii) Fill in the first column with the time (in minutes) of the samples recorded for the background
 - iii) In the 'Fluor' column, take the average of the samples recorded for respective time interval sample range marked by the events.
 - iv) In the '*t0 removed*' column, fill in the difference between the average measurement for the 0 minute time sample and the raw fluorescence for each sample.
 - v) The 'microM' column will use the result of the standard curve slope.
 - (1) Divide the '*t0 removed*' column value by the slope of the standard curve to determine the corresponding μM concentration of H_2O_2 value
 - vi) The 'nmol' column is H_2O_2 equivalent and is found by multiplying the 'microM' column by 25 (mL).
 - vii) Plot column 5 vs. column 1 as a scatter plot.
 - viii) Add trend line
 - (1) Select set intercept to (0,0)
 - (2) Select display equation on chart
 - ix) Use the slope as the rate of autoxidation in nmol increase in H_2O_2 per minute to be removed from experimental data
- 4) Lung data processing
- i) Write a row with the following column headings

(1) time of sample, raw fluorescence measurement, background measured at time 0 removed, concentration of H₂O₂ in μ M, nmol of H₂O₂ measured with background increase in fluorescence, nmol of H₂O₂ corrected from the rate of background increase in fluorescence, and nmol of H₂O₂ per gram of DLW

Time	Fluor	T=0 remov	microM	nmol	nmol-BG	nmol/g
0	518059	0	0	0	0	0
10	1043969	525910.1	0.649346	16.23366	11.92833	48.88658
20	1637708	1119649	1.382442	34.56105	25.95038	106.354
30	2138841	1620782	2.001195	50.02987	37.11387	152.106

- ii) In the 'Fluor' column, take the average of the samples recorded for respective time interval sample range marked by the events.
- iii) For the 'T0 removed' column, set the column equal to the raw fluorescence column minus the first raw fluorescence measurement.
- iv) The 'microM' column is the value of the corrected fluorescence values divided by the slope determined from standard curve data processing.
- v) The 'nmol' column is the product of the concentration (column 4) and 25.
- vi) To account for background autoxidation, the product of the time (column 1) and the rate of autoxidation (nmol/min) determined in the background analysis is removed from the nmol determined in column 5 for each row.
- vii) The normalized data in the 'nmol/g' column is the value in column 6 is divided by the dry lung weight measured after it the lung is fully dried.
- viii) Plot column 7 vs. column 1 as a scatter plot
- ix) Add trend line
 - (1) Select set intercept to (0,0)

- (2) Select display equation on chart
- (3) If there are other conditions tests that do not start at 0 min, do not select set intercept to (0, 0). Record the slope displayed for the range selected for the given condition.
 - x) Use the slope as the rate of production of ROS production (nmol/g/min).
- 5) Record rates in a master copy for all experiments for future reference and data processing.